AN INVESTIGATION ON THE AERODYNAMIC PERFORMANCE OF A VERTICAL AXIS WIND TURBINE

By

ETESH VAISHNAV

Bachelor of Science in Mechanical Engineering
Bhilai Institute of Technology
Durg, India
2007

Submitted to the Faculty of the
Graduate College of
Oklahoma State University
in partial fulfillment of
the requirements for
the Degree of
MASTER OF SCIENCE
December, 2010

AN INVESTIGATION ON THE AERODYNAMIC
PERFORMANCE OF A VERTICAL AXIS WIND TURBINE

Thesis Approved:

Dr. Khaled A. Sallam

Thesis Advisor

Dr. Andrew S. Arena

Dr. Frank W. Chambers

Dr. Mark E. Payton

Dean of the Graduate College

ACKNOWLEDGMENTS

I would like to express my gratitude to my mentor Dr. Khaled A. Sallam for his invaluable guidance. Without his advice this thesis would not have been possible.

I also would like to gratefully acknowledge my hearty appreciation to my advisory committee: Dr. Frank W. Chambers and Dr. Andrew S. Arena.

I am forever indebted to my parents for their endless patience, encouragement and love when it was most required. I owe a debt of gratitude to my girlfriend, Niraja Singh, for her countless support. Khushwant Saini, Vivek Dubey, Rohit Pillay and Siddarth Agrawal, I am privileged to have such roommates helping me at all moments.

I am also thankful to all those people who are directly or indirectly associated with me and whose contribution made this project attain a successful completion.

TABLE OF CONTENTS

LIST OF TABLES

LIST OF FIGURES

NOMENCLATURE

C_L	Lift coefficient
A	Frontal area of wind turbine [m^2]
C_D	Drag coefficient
C_m	Moment coefficient
C_p	Power coefficient
D_θ	Tangential component of drag
D_R	Radial component of drag
F_θ	Total tangential force
F_R	Total radial force
L_Θ	Tangential component of lift
L_R	Radial component of lift
P	Power [watt]
p	Pressure [atm]
R	Length of the rotor arm [m]
Re	Reynolds number
t	Time [sec]
T	Temperature [Kelvin]
T	Torque [N-m]
V	Wind velocity [m/s]

Greek Symbols

ρ	Air density

α	Angle of attack
Ω	Angular velocity [radian/s]
μ	Dynamic viscosity [N-s/m^2]
k	Kinetic energy
θ	Rotational angle of airfoil
λ	Tip speed ratio
ε	Turbulence dissipation rate

ABBREVIATIONS

AR	Aspect Ratio
CFD	Computational Fluid Dynamics
DES	Detached Eddy Simulation
DNS	Direct Numerical Simulation
LES	Large Eddy Simulation
NSE	Navier Stokes Equation
RANS	Reynolds Averaged Navier Stokes
RNG	Renormalization Group
S-A	Spalart Allmaras
S k-ε	Standard k- ε
SST K- Ω	Shear Stress Transport K-Ω

CHAPTER 1

INTRODUCTION

1.1 General Statement of The Problem

1.1.1 Background

Non-renewable resources of energy are limited in the world and are depleting at a faster rate due to rapidly growing population. These energy resources are exhaustible and are the main cause of pollution, which is eventually leading to another major problem of global warming. Considering all these problems, it has now become a dire need to find another substitute of energy which is mainly pollution free and available in abundance. Among all the available renewable energy resources, wind energy has many advantages like it is available in abundance, does not contribute to global warming, requires less installation and maintenance cost for power generation. The top leading countries in the field of wind energy production are USA, China, Spain and Denmark. For many years wind energy has been used for many small purposes like for water pumping with the capacity of 10 - 250 kW and for producing mechanical power to operate some small devices, but nowadays it is also being used to produce electricity with the application of wind turbines. Wind turbine consists of a rotor shaft and a generator mounted in a nacelle.

Based on axis of rotation, wind turbines are divided into two types: Horizontal axis wind turbines (HAWT) and vertical axis wind turbines (VAWT). In case of horizontal axis wind turbines (HAWT), this arrangement is mounted at the top of a tower with the rotor blades facing the wind directly. Whereas in case of VAWT, this

arrangement is mounted vertically hence provides better stability to rotor blades and are easily accessible for maintenance. Apart from having this arrangement, rotor of VAWT requires no yaw mechanism to maintain a proper stability. VAWT is further divided into lift driven VAWT (Darrieus type) and drag driven VAWT (Savonius type) as shown in figure 1.1 and figure 1.2 respectively. Darrieus type VAWT proves to be more efficient than Savonius type turbine. G. J. M. Darrieus was the first to come up with an invention of VAWT in 1931 and since then study of wind turbine has been of interest to many researchers. Figure 1.5 provides a statistical data of world wide installed capacity of wind energy in MW.

After mid 80s, there has been a renaissance of interest regarding sources of renewable energy among numerous researchers (Bragg and Schmidt, 1978; Marini et al., 1992; Wang, 2000; Chen and Zhou, 2009; Claessens, 2009; Ferreira, 2009) carrying out extensive studies in the field of wind turbines. These studies have led to a wide range of designs of VAWT and suggested various improvements on a conceptual basis. Selection of a wind turbine depends on the required tip speed ratio for instance, straight bladed-VAWT is generally suitable to operate at high λ to avoid the problem of self-starting, whereas helical type VAWT as shown in figure 1.3 is generally suitable to operate at comparatively lower value of λ.

Various authors investigated the performance of VAWT, mainly including Bragg and Schmidt (1978), Cetin et al. (2005) and Ferriera (2009) to name a few. Figure 1.6 by Bragg et al. (1978), depicts a curve between C_p and λ for varieties of wind turbines. With this figure he explained the efficiency limit of an ideal wind turbine, first proposed by a German physicist Betz in 1919, according to him no wind turbine can have its efficiency (i. e. C_p) more than 0.59 and this limit is called Betz limit. Figure 1.7 shows a study by Chen and Zhou (2009) which explains the effect of pitch angle on a performance of VAWT. Claessens (2009) in his thesis investigated the effect of airfoil thickness on C_p of a wind turbine as shown in figure 1.8.

1.1.2 Problem Statement

The present study explores a range of factors influencing the aerodynamic performance of a VAWT. The effect of tip speed ratio has been examined which is considered to be a prominent factor in deciding C_p of a wind turbine. In this regard, λ is optimized for the maximum efficiency of the turbine. Effect of rotor diameter on C_p has also been a part of this study. Furthermore, the blade and tower wakes at low and high Reynolds numbers and their effects on C_p has also been the area of concern in the present study. In addition, present study elucidates the effect of solidity on C_p of a VAWT.

1.2 Previous Related Studies

1.2.1 VAWT

The research on VAWT aerodynamics began with the stream tube momentum model and vortex model. There are many factors that affect the propulsive performance of an airfoil like angle of attack, tip speed ratio, thickness, symmetricity of an airfoil, lift and drag coefficient. While designing a quasisteady model of an airfoil these factors were not taken into consideration hence the model did not come out to be a more practical model. Therefore, studies of flapping and plunging airfoil, mainly by Sane et al. (2002), Lee et al. (2006) and Shyy et al. (2009) came into existence where the forces acting due to the unsteady motion of a wing were calculated.

Guerri et al. (2007) and Chen and Zhou (2009) both analyzed the flow around a rotating VAWT by using Reynolds Averaged Navier Stokes (RANS) solver in 2-D simulation. PISO discretization scheme with SST K-ω model was used to get the flow details near the wall of the blades. Sliding mesh technique was used to make a moving mesh. NACA 0018 airfoil type was chosen for both the studies. Grid was split into moving and rotary part. Guerri et al. (2007) calculated the horizontal

and vertical component of the forces acting on the airfoil to determine the value of the total torque generated by VAWT whereas Chen and Zhou (2009) reported the coefficient of moment. Moment coefficient of an airfoil is calculated by the following formula:

$$\mathrm{C}_m = T_{mean}/0.5\rho \mathrm{A} V^2 \mathrm{R} \tag{1.1}$$

Chen also investigated the effect of pitch angle on VAWT aerodynamic performance and obtained an optimum range of pitch angle which would give maximum power output keeping tip speed ratio constant. Figure 1.7 shows the variation of C_p with pitch angles. Guerri et al. (2007) analyzed the influence of tip speed ratio on the aerodynamic performance of VAWT and also showed that the resulting value of C_p obtained with RANS simulations is more accurate as the same C_p can be achieved at relatively lower value of λ than obtained with the Multiple Stream Tube theory. He also found that the computed force and torque vary periodically as a function of angle of rotation θ.

Howell et al. (2009) and Claessens (2006) performed experimental and computational studies on 2-D and 3-D models at different Reynolds numbers. He obtained 3-D computational results in a good agreement with the experiments. Effect of surface roughness was also taken into consideration. It was concluded that 2-D CFD results are always higher than 3-D CFD results and this is because of the presence of end tip vortices which causes circulation in real wind turbine. In case of 2-D, losses due to the end tip vortices and rotor arm are ignored. Periodic pattern of coefficient of moment was also observed with three cycles per revolution. Claessens (2006) studied the effect of Reynolds number, airfoil thickness and tip speed ratio on NACA 0012, NACA 0015, NACA 0018, and NACA 0021. Figure 1.8 by Kirke and Lazauskas (1991) shows the influence of airfoil thickness on the turbine performance at Re = 200000.

Tang et al. (2007) studied the effect of structural flexibility of airfoils on the

fluid flow pattern around the VAWT. They found that structural flexibility causes pitching and heaving motion to an airfoil when it comes to the effect of aerodynamic forces. This leads to significant changes in lift and thrust generation as explained in the previous equation, hence propulsive performance of a VAWT. Geometry of an airfoil is also an important factor that influences aerodynamic performance and cost of the wind turbines. Marini et al. (1992) studied the different airfoil shaped blade of a VAWT and their performances. They used Single stream-tube momentum model and free wake vortex model for their experiments. Ferreira (2009) did a study on 2-D and 3-D wake generation of VAWT.

1.2.2 Flapping Wings

Hover et al. (2004) have conducted studies on angle of attack profiles and their influences on propulsive performance of a plunging and flapping airfoil. They employed the method given by Read et al. (2003) that involved the comparison of performances obtained by four different types of angle of attack profiles. The principle behind their investigation was to vary the angle of attack to achieve a desired profile so as to get the enhanced thrust performance. Shape of the angle of attack profile affects the wake pattern hence the coefficient of thrust. Thrust coefficient of an airfoil is calculated by the following formula:

$$\mathrm{C}_{thrust} = F_\theta / 0.5\rho \mathrm{A} V^2 \tag{1.2}$$

Where F_θ is the tangential force acting on airfoil.

Four major lift generating mechanism used by birds and insects have been identified by Ellington et al. (1996) and then experimentally confirmed by Tang et al. (2007). Computational model proposed by Wang (2000) to solve Navier-Stokes equation for two-dimensional plunging airfoil proved to be very significant contribution when it was compared with the results obtained by Birch and Dickinson (2001). Inves-

tigations have been made by Lee et al. (2006) on unsteady, viscous and incompressible flows over a two dimensional flapping airfoil.

Tay and Lim (2009) considered several variables like Strouhal numbers, pitch amplitude and phase angle to evaluate lift, thrust and efficiency of non-symmetrical flapping airfoil. They found that lift force depends on the shape of the airfoil whereas thrust force depends on variables.

Strouhal number is a dimensionless parameter which describes the flapping flow mechanism and is given as:

$$\mathrm{S}_t = \frac{fL}{v} \tag{1.3}$$

Where:

f = Frequency of vortex shedding

L = Characteristic length (Chord length in present case)

V = Velocity of the fluid

Symmetrical airfoil contributes to only thrust and propulsive efficiency not to lift whereas non-symmetrical flapping airfoil not only gives high thrust and efficiency but high lift also. Sane and Dickinson (2002) modified quasi-steady model of a flapping flight. They compared rotational force produced by hovering insect wing rotating at a certain angular velocities with the force produced by translation of the wings of quasi-steady model. Birch and Dickinson (2001), Ansari et al. (2006), Shyy and Liu (2007), Shyy et al. (2009) conducted studies on Leading edge vortex phenomena of a flapping wing of an insect to improve the aerodynamic performance. Dynamic stall is a mechanism that gives rise to leading edge vortex (LEV) which is accountable for a good performance of flapping wings. This LEV detaches from the wing and forms wake into the trailing edge. Ansari et al.'s (2006) study was focused on complex interaction between leading edge vortex (LEV) and trailing edge vortex (TEV). Shyy and Liu (2007) explained that both the phenomena pressure gradient and centrifugal force in the momentum equation cause to generate LEV. They utilized results ob-

tained from experiments conducted by Birch and Dickinson (2001) on insect flying at low Reynolds number and concluded that reduction in effective angle of attack considerably reduces the effect of downwash and hence reduces the growth of LEV. Shyy et al. (2009) demonstrated that having a low aspect-ratio of a flapping wing can increase lift even if the wing is surrounded with the tip vortices. Lee et al. (2006) successfully proposed a theory that thrust and drag generation depends on leading and trailing edge vortex.

Numerous aspects of an aerodynamic performance of VAWT have been questioned throughout the literature concerning the performance optimization of wind turbines. Plenty of literatures are available dealing with the performance optimization of wind turbines at high Reynolds number above 10^6 whereas very few are available concerning low Reynolds number flow especially for Laminar flow. This brings upon a need for further investigations into Laminar flow regimes over VAWTs. The effect of solidity on C_p was not in a preview of available literature which makes it an immediate need to explore about. Therefore, in a view of current status concerning an aerodynamic performance of VAWT, present study is extended to improve upon the conceptual approach.

1.3 Specific Objectives

Review of literature suggested the following specific objectives to accomplish in the present study:-

- To investigate the aerodynamics of a moving airfoil (NACA0018) of VAWT in two dimensional unsteady flows at Reynolds number of 1.086×10^6 using ANSYS FLUENT 12.0.16 for simulation and ICEM CFD to generate sliding mesh.

- To study the variation of performance coefficient of VAWT at different tip speed ratios and obtain an optimum value of tip speed ratio (λ) at which VAWT

produces maximum power output for NACA 0018 airfoil.

- To investigate the influence of rotor diameter on aerodynamic performance of VAWT.

- To study the effect of laminar boundary layer separation on C_p of a VAWT by comparing the results of Laminar viscous model and RANS turbulence model.

- To consider the effect of solidity (which is given by $\sigma = N_b C/R$) on VAWT's performance at $\sigma_1 = 0.321$ for three bladed VAWT and $\sigma_2 = 0.642$ for six bladed VAWT.

1.4 Organization of The Thesis

The thesis is organized into four chapters. The statement of the problem, specific objectives of the present study and literature review have been presented in the first chapter. The second chapter describes the computational methods used during the present study. The results and discussions are presented in the third chapter. Finally, the summary and main conclusions of the present study, including recommendations for future study, are presented in the fourth chapter.

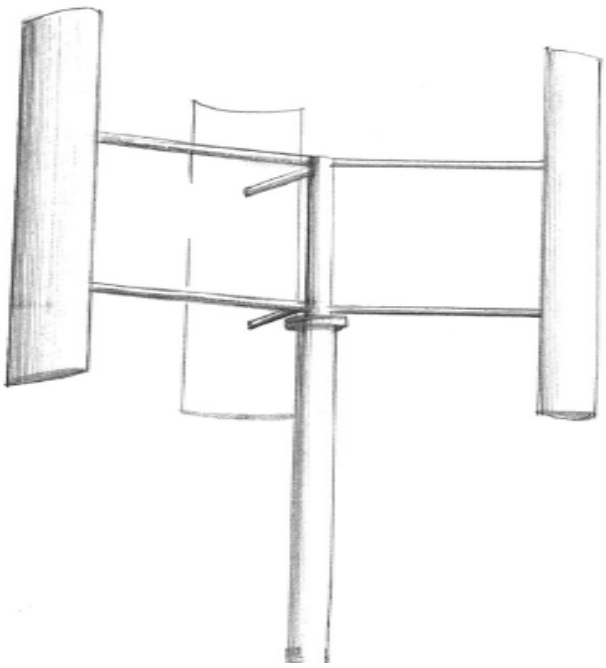

Figure 1.1: Darrieus type straight bladed VAWT (Islam et al., 2006).

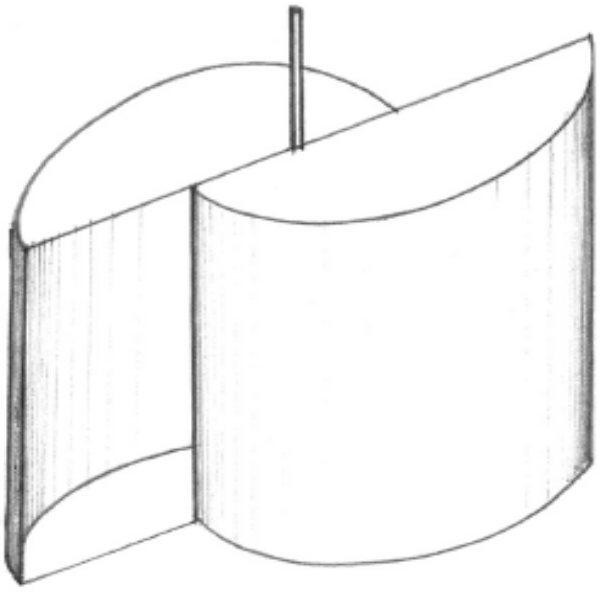

Figure 1.2: Savonius type VAWT (Islam et al., 2006).

Figure 1.3: Helical type VAWT (Quiet Revolution Ltd, 2008).

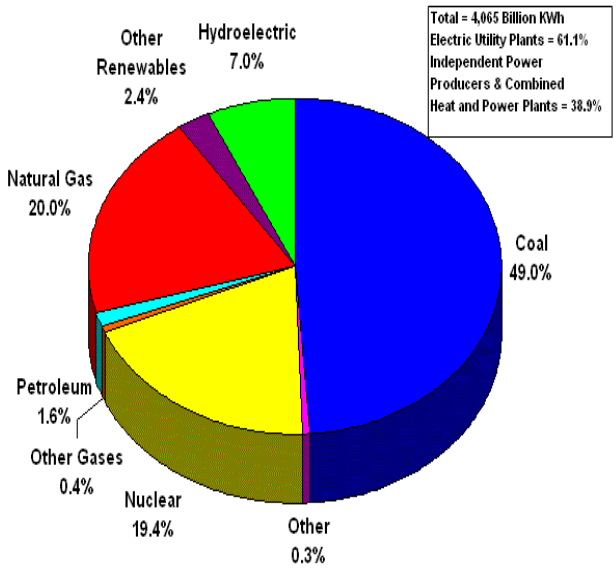

Figure 1.4: Worldwide electrical power generation (World Wind Energy Report, 2008).

Figure 1.5: Installed capacity of wind energy on yearly basis (World Wind Energy Report, 2008).

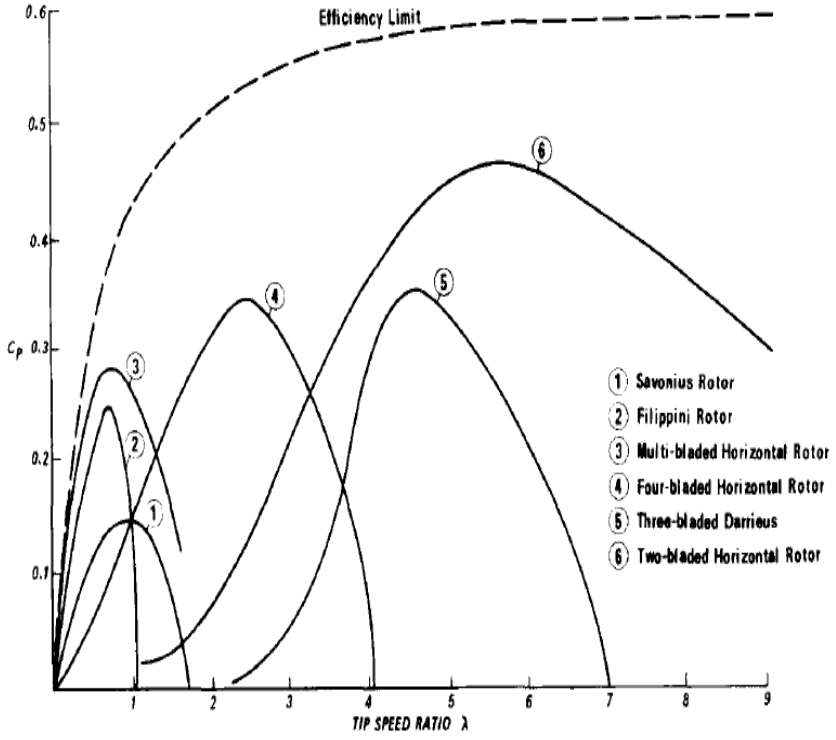

Figure 1.6: C_p-λ curve for various types of wind turbines (Bragg and Schmidt, 1978).

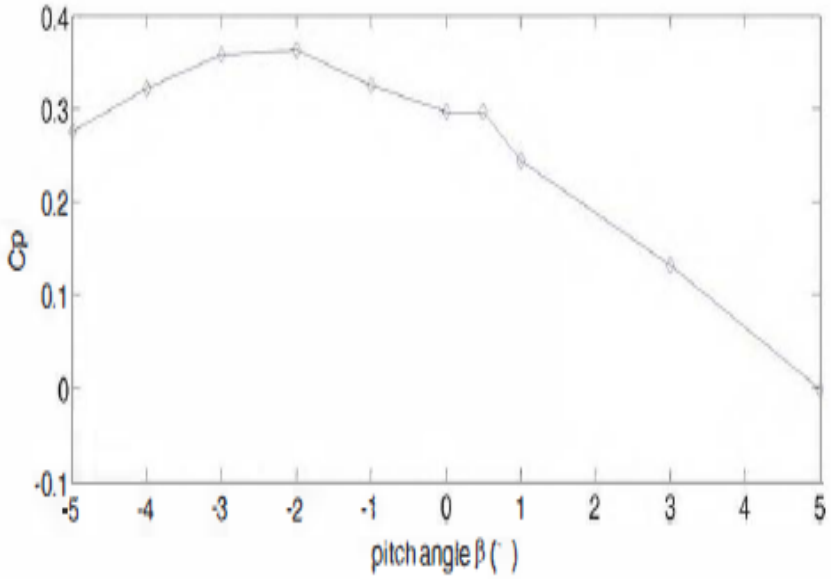

Figure 1.7: Variation of C_p with pitch angles at $\lambda = 4$ (Chen and Zhou, 2009).

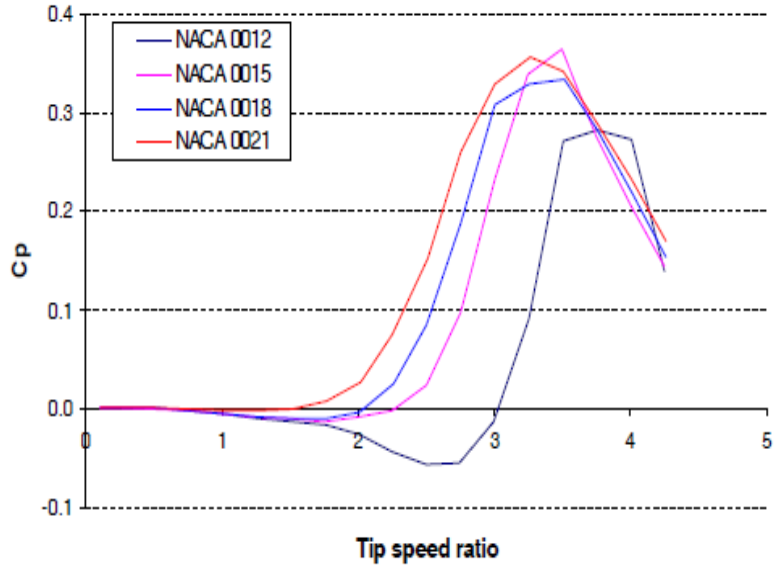

Figure 1.8: Influence of airfoil thickness on VAWT's performance at Re=200,000, V=10 m/s [Kirke and Lazauskas (1991), Claessens (2006)].

CHAPTER 2

COMPUTATIONAL METHODS

2.1 Introduction

The governing equations in Computational Fluid Dynamics (CFD) basically consist of Continuity Equation, Conservation of Momentum also known as Navier-Stokes Equation and Conservation of Energy. Fluent deals with inviscid and viscous flow both, but in the present study we are dealing with the viscous flow; therefore, Continuity Equation and Navier-Stokes Equation will be mainly the area of concern. Some of the prominent advantages of using CFD methods include the accuracy and reliability of the results and lower cost of application of CFD as compared to the expensive experimental methods. CFD uses computational software which offers a user-friendly platform that enables users to simulate any flow with various sets of test conditions.

CFD works on a principle of discretization where a flow domain is discretized in very small units called cells. This unit cell structure is known as mesh or grid. Several discretization schemes are available in Fluent and choices can be made on the basis of the needs of the end result. These cells are used for the analysis of the flow problem. Fluent gives the properties of the fluid at every single node. Spatial discretization schemes available in Fluent are Least Squares Cell based, Green Gauss Node and Cell based which is to be chosen according to the flow pattern. A pre-processing is required before proceeding to the post-processing. ICEM CFD has been used as a pre-processor to generate the sliding mesh and FLUENT as a post-processor for the simulation process. In addition to this, the boundary condition of the problem is one of the decisive factors that plays a vital role in determining the accuracy of

the simulation process. Therefore, it is the matter of great importance to select an appropriate boundary condition so as to achieve a desired result.

This chapter provides a detailed explanation of various parameters used to set up the simulation of a fluid flow around a two dimensional rotating VAWT using NACA 0018 airfoils. This chapter deals with the types of viscous model, boundary conditions, discretization schemes, time step calculations, reference values and solver used. The grid is generated using ICEM CFD and flow is analyzed using FLUENT. Numerical values of forces obtained from the simulation are validated with the research article by Guerri et al. (2007) by plotting a graph between force and angle of rotation. Another validation is made by comparing a graph between C_p and λ obtained by CFD computations, with the experimental results by Claessens (2006).

2.2 Governing Equations

Computational Fluid Dynamics comprise the governing differential equations and applicability of these governing equations depend on the nature of the flow. These equations have their mathematical representations which can be employed individually or in a group depending on the need of the desired output. Three basic principles which govern the characteristics of the flow of any fluid are conservation of mass, momentum and energy. In present case, we are dealing with the equation of continuity with the application of K-Ω model.

The Continuity Equation or Conservation of Mass given by White (2005), as follows:

$$\frac{\partial \rho}{\partial t} + \frac{\partial \rho u}{\partial x} + \frac{\partial \rho u}{\partial y} + \frac{\partial \rho u}{\partial z} = 0 \tag{2.1}$$

Navier-Stokes Equation for an incompressible flow given by White (2005), as follows:

$$\rho \left[\frac{\partial u_i}{\partial t} + \frac{\partial u_k u_i}{\partial x_k}\right] = -\frac{\partial \rho}{\partial x_i} + g_i + \mu \frac{\partial^2 u_i}{\partial x_k x_k} = 0 \tag{2.2}$$

2.3 Geometry of NACA 4 digit series

NACA 4 digit airfoil family is defined by a series of numbers where each number has its own significance, for instance in NACA 0018 the first digit represents maximum camber as percentage of chord and it is denoted by 'm'. Second digit refers to distance of maximum camber from the leading edge in tenth of percentage denoted by 'p'. Rest of the two digits designate to maximum thickness of airfoil as a percentage of chord denoted by 't'. Coordinates of NACA 0018 airfoil used for the present study has been listed in Appendix (B). The coordinates of NACA 4 digit airfoil family are given by the following equations as mentioned by Abbott and Doenhoff (1959):

$$\text{y} = \frac{tc}{0.2}[0.2969\sqrt{x/c} - 0.1260(x/c) - 0.3516(x/c)^2 + 0.3516(x/c)^3 - 0.3516(x/c)^4] \tag{2.3}$$

Where:

c is the chord length of the airfoil

x is the position along chord from 0 to c

y is the half thickness at a given value of x

t is the maximum thickness as a fraction of chord

The position of the coordinates on the upper curve of the airfoil (X_U, Y_U) and lower curve (X_L, Y_L) of the airfoil is given by

$$X_U = X_L = \text{X} \tag{2.4}$$

Similarly, the position of the coordinates on lower curve of the airfoil (X_L, Y_L) is given by:

$$Y_U = +\text{Y} \tag{2.5}$$

$$Y_L = \text{-Y} \tag{2.6}$$

2.4 Geometry Creation

ICEM CFD has been used as a pre-processor for the grid generation. Symmetrical airfoil NACA 0018 has been used for the present study as shown in figure 2.3. Rotor is equipped with three airfoils each with the chord length of 0.107 m. located at 120° from one another. Diameter of the rotor is set as 2 m. and far-field is located at 168 chords from the center of the rotor. Formatted point data for airfoil come from different sources. For this case NACA ASCII 4 digit series has been used. Two curves with 100 node points on each of them is drawn using create/modify tool going all the way from leading edge to trailing edge. All the curves and surfaces are assigned separately with different part names, this helps setting up the boundary conditions distinctly.

2.5 Grid Generation

Two separate zones are created, rotor being rotary and square far-field being stationary. The far-field mesh which is of hexahedral type is less dense as compared to hexahedral mesh in the rotary zone. 2-D planar blocking is created around the 120° section of rotor as depicted in figure 2.4. Having a proper edge-curve association helps get a nice fit of mesh around the edges. Among several types of grids available in ICEM CFD like H-grid, O-grid, C-grid and Y or quarter O-grid, current meshing uses quarter O-grid along with the C-grid around the airfoil. O-grid allows a uniform orientation of mesh around the geometry and C-grid captures the geometry of the airfoil as illustrated in figure 2.6. Block is then split to capture the airfoil geometry. Blades of the vertical axis wind turbine are set to rotate by making a pair of opposite nodes periodic. This is done by setting up base, axis and angle in global mesh parameters and then selecting periodic vertices using the edit block tool. Hexahedral

meshing is used considering the fact that hexahedral mesh provides more uniform and smooth meshing over tetrahedral or quad. Edge meshing parameters are used to get a more uniform mesh distribution. Mesh around the airfoil needs to be dense enough so as to have a smooth gradient change in fluid. Figure 2.5 shows the schematic view of the hexahedral meshing of 120° section of a rotor. This 120° section is then copied and rotated to get a complete 360° VAWT as shown in figure 2.7. FLUENT does not accept structured mesh pattern therefore, the structured hexahedral mesh is converted into unstructured mesh before exporting it to FLUENT. Figure 2.8 shows the complete set up of a VAWT mesh.

2.6 Turbulence Model

The end result of the flow problem primarily depends on the Reynolds number. Working with high Reynolds number is comparatively complex as it requires more precision and accuracy to deal with. Computational Fluid Dynamics offers a gamut of flow models which can be used individually as per the requirement of the end result. Various turbulent modeling and simulation techniques like Direct Numerical Simulation (DNS), Large Eddy Simulation (LES), Detached Eddy Simulation model (DES), Reynolds Stress Model (RSM), K-ϵ model, K-ω model, Spalart-Allmaras model are available and each one of them can be effectively used in particular area of applications.

In the present study, wall bounded turbulent flows around the vertical axis wind turbine has been modeled using SST K-ω model. SST model for K-ω differs from standard model in a context that SST provides a change in a gradual manner from standard K-ω model in the inner region to high Reynolds number flow with K-ϵ model in the outer region. In order to achieve this, K-ϵ model is transformed into a K-ω formulation. Two equation eddy viscosity turbulence model by Menter (1994) is given by these equations:

$$\frac{\partial(\rho k)}{\partial t} + \frac{\partial(\rho u_j k)}{\partial x_j} = \text{P- } \beta * \rho\omega \text{ k} + \frac{\partial[(\mu+\sigma_k\mu_t)\frac{\partial k}{\partial x_j}]}{\partial x_j} \tag{2.7}$$

$$\frac{\partial(\rho k)}{\partial t} + \frac{\partial(\rho u_j k)}{\partial x_j} = \frac{\gamma}{\nu_t}\text{P - } \beta\rho\omega^2 + \frac{\partial[(\mu+\sigma_\omega\mu_t)\frac{\partial \omega}{\partial x_j}]}{\partial x_j} + 2(1-F_1)\frac{\rho\sigma_\omega}{\omega}\frac{\partial k}{\partial x_j}\frac{\partial \omega}{\partial x_j} \tag{2.8}$$

2.7 Boundary Conditions

Boundary condition in Fluent defines the flow parameters at the boundaries of the flow domain. The end result depends on the boundary condition to a great extent. There are various boundary types available in FLUENT like pressure inlet, velocity inlet, mass flow inlet, pressure outlet, pressure far-field, outflow, stationary wall, moving wall and axis. In our current study, periodic boundary condition is applied to set the airfoils rotating. Boundary conditions used for the present case have been shown in figure 2.8.

In order to use velocity inlet as a boundary type the magnitude and direction of the velocity must be known. The possible pairs of boundary types at the inlet and exit are:

Pressure inlet - Pressure outlet

Mass flow inlet - Pressure outlet

Velocity inlet - Pressure outlet or Outflow

For our study a boundary pair of velocity inlet and outflow is used. Outflow boundary condition is generally suitable for the simulation of airfoil related problems. Airfoils are considered to be a stationary wall in reference to a moving fluid zone.

2.8 Problem Set up in Fluent

Rotating hexahedral mesh of the rotor is merged with the stationary mesh of the far-field. Mesh is then checked into ICEM CFD for all possible errors like uncon-

nected vertices, periodicity, uncovered faces and single elements. ANSYS is used as a common structural solver and Fluent_V6 as an output solver to write a mesh file which could be read into FLUENT. Two dimensional double precision solver with parallel processing option is used. Mesh is checked again in Fluent for any negative volumes and skewness. FLUENT also allows scaling the size of the working domain and at the same time the user can set the units in SI, CGS and other format. In order to apply periodicity turbo-outer and far-inner both the parts are changed from wall boundary types to interface boundary types. Now mesh interface is created by selecting both the interface zones which allows us to set the rotational periodic boundary conditions. Moving mesh technique is applied for this simulation where rotor is set to rotate at 380 RPM but the far-field remains stationary. Various types of pressure velocity coupling schemes are available in FLUENT and their selection depends on various factors. The present study involves the application of SIMPLE scheme. Among several special discretization schemes available in FLUENT, Green-gauss node based gradient with Presto pressure and second order upwind scheme are found to be appropriate for the present study. Simulation begins with first order upwind scheme and then continues with the second order after the first convergence is reached just to avoid instability in flow. Convergence criterion for the solution are set as 10^{-6}. Appendix (A) describes the steps followed in FLUENT for a flow modeling of VAWT. Currently, our area of consideration is to determine the forces acting on each of the three rotating airfoils and to obtain an optimum value of tip speed ratio which gives the maximum power output when wind passes the turbine at a speed of 10 m/s. In the present study Reynolds number is set as 1.086×10^{6} for a rotor diameter of 2 m. In the present case Reynolds number based on rotor diameter (D) is given by:

$$Re_D = \frac{\rho V D}{\mu} = \frac{1\times10\times2}{1.8421\times10^{-5}} \tag{2.9}$$

2.9 Time Step Calculations

Unsteady simulation involves time dependent calculations. Time step is calculated using speed of the rotor.

Rotational speed of the rotor N = 380 rpm = 380/60 revolution/sec = 6.33 rps

Or, Rotor makes 6.33 revolutions in one second

Or, it takes 0.1579 seconds to make 1 revolution or (360°)

Therefore, time taken to rotate 360° is 0.1579 seconds

Time step size is given as 1.052×10^{-4} seconds

Therefore number of time steps required for one revolution

$= 0.1579/1.052 \times 10^{-4} = 1500$ time steps

Maximum iterations per time step = 80

The maximum iterations per time step in FLUENT basically sets the maximum number of iterations to be performed per time step, which is generally used for unsteady flow calculations. If the convergence criteria are achieved before this particular number of iterations is performed, the solution moves to the next time step.Therefore it is recommended to set the value of maximum iterations per time step little high.

2.10 Reference Values

Chord length = 0.107 m

Reference Length = Radius of The Rotor = 1 m.

Area = Rotor Diameter× span = 2*1 = 2 m^2 for 2-D Span = 1

Enthalpy = 0 jule/kg

Pressure = 1 atm at the Velocity Inlet

Density = 1 kg/m^3

Temperature = 288.16 k

Reynolds number = 1.086×10^6

Viscosity = 1.8421×10^{-5} kg-s/m

Turbulent Kinetic energy = 1.5 $m^2/\ s^2$

Turbulent dissipation rate = 1386 s^{-1}

2.11 Airfoil Lifting Theory

Blades of a wind turbine is considered to be like an airfoil therefore, the same airfoil lifting theory is applied to the blades of a wind turbine as well. Mechanism of lift generation in airfoil is based on Bernoulli's principle, (White, 2005) which states that velocity of the fluid increases where the pressure generated by the fluid decreases or vice versa. This phenomenon causes lift to generate on airfoil. The velocity of the wind passing over the upper surface of the airfoil is more than the one passing over the lower surface and according to Bernoulli's principle, pressure on the lower surface is more than the pressure on the upper surface which causes a pressure difference and this whole mechanism eventually leads to an aerodynamic lift generation. In case of wind turbines, this aerodynamic lift causes rotation of the turbine blades.

2.12 Tip Speed Ratio

Tip speed ratio is an important factor that affects power output of a wind turbine greatly. Proper attention must be paid while designing a wind turbine so as to achieve an optimum tip speed ratio. Angle of attack of blade varies as the turbine rotates. Angle of attack is inversely proportional to the tip speed ratio. Therefore, at higher tip speed ratio a blade experiences lower angle of attack leading to lower stall creation. For a tip speed ratio of above 3 the stall produced by turbine is very low hence positive torque is generated. Torque generation also depends on the type of airfoil chosen and Reynolds number. According to Betz limit (Cetin et al., 2005) no wind turbine can have its efficiency more than 0.593. Tip speed ratio is a ratio of linear velocity of the blades to the free stream velocity of the wind. It is a dimensionless parameter which

is defined as:

Tip Speed Ratio λ = linear velocity of the rotor blade/wind velocity

$$\lambda = \omega \times \mathrm{r}/\mathrm{V} \tag{2.10}$$

where:

λ = Tip Speed Ratio

ω = Angular velocity of rotor blade

r = Rotor radius

V = Wind velocity

2.13 Angle of Attack

Angle of attack α, is defined as the angle subtended by an oncoming wind velocity with the chord line of an airfoil. The angle of attack depends on the rotational angle θ and tip speed ratio λ which is given as:

$$\alpha = \tan^{-1}[\tfrac{cos\theta}{\lambda - sin\theta}] \tag{2.11}$$

As the blade rotates angle of rotation also changes and it causes a change in angle of attack. As it is shown in figure 2.2, α increases gradually for a range of θ = 0 - 45 then it decreases and goes negative from 45 - 60 and then increases between 60 - 225. A condition of stall occurs after α reaches 40 degrees where drag force becomes dominant over lift force.

2.14 Von Karman Vortex Street

Figure 2.15 (b) shows a phenomenon in fluid dynamics. When fluid flows over a cylindrical body it creates periodic pattern of swirling flows which is called Von Karman Vortex Street. This wake shedding is the result of a flow separation usually occur at low Reynolds number. Leading and trailing edge vortex formation is depicted

in figure 2.14 and figure 2.15 (a). The velocity vectors at V_∞ = 10 m/s, over the surface of the airfoil, at the outflow, leading edge and trailing edge is also shown in figure 2.10 - figure 2.13 respectively.

2.15 Calculation of Torque Produced by Horizontal and Vertical Forces Acting on Airfoils

Forces acting on each airfoil are sum of the two components that is pressure force and viscous force. In order to calculate the torque produced by each airfoil, this force is further split into horizontal and vertical direction. Component of these two forces do not always contribute to the torque due to the rotary motion of the turbine. The component of force for which axis of rotation of turbine lies in its direction, produces no torque. Forces acting on each airfoil are set to be reported in FLUENT in horizontal and vertical direction. The component of these forces in horizontal and vertical direction obtained by using data sets by Guerri et al. (2007) is illustrated in figure 2.16 and figure 2.18 respectively. Torque produced by each airfoil is then calculated by following equations:

$$\text{T1} = \text{- Fx1.Rcos}\,\theta \text{ - Fy1.Rsin}\,\theta \tag{2.12}$$

$$\text{T2} = \text{- Fx2.Rcos}\,(\theta + 120) \text{ - Fy2.Rsin}\,(\theta + 120) \tag{2.13}$$

$$\text{T3} = \text{- Fx3.Rcos}\,(\theta + 240) \text{ - Fy3.Rsin}\,(\theta + 240) \tag{2.14}$$

$$\text{Total Torque T} = \text{T1} + \text{T2} + \text{T3} \tag{2.15}$$

(Total Torque 'T' is calculated for every 6 degrees of rotation)

$$\text{Average Torque} = \sum \text{T/n} \tag{2.16}$$

where n is number of recorded values = 360/6 = 60

2.16 Grid Independence

Computational results obtained by CFD simulation must be grid independent. The results should not vary with the number of cells in mesh. Therefore, grid independency is one of the important parameters to check the accuracy of the solution. Simulation is run for a cell size of 65000 and 140,000 and then component of the forces are plotted as a function of angle of attack. Results are found to be independent of the number of cells with negligible difference in their magnitude. Figure 2.16 and Figure 2.18 shows the grid independent solution obtained by simulations. These graphs also serve the purpose of validation as figure 2.16 and 2.18 follows the same trend as shown in figure 2.17 and 2.19 by Guerri et. al (2007).

2.17 Validation of 2-D CFD simulation

Simulation is set to run at several tip speed ratios ranging from 1- 6 at Reynolds number of 10^6 and then a graph is plotted between C_p and λ. Results are found to be in a good agreement with the experimental result by Claessens (2006) as shown in figure 2.20. Maximum $C_p = 0.34$ is obtained at $\lambda = 3.8$.

Table 2.1: Data sets used for simulation in FLUENT ($V_\infty = 10$ m/s, Rotor Diameter = 2 m.)

TSR	Speed in RPM	Total Time Steps	Step Size δt	Total Time/cycle	Cp(obtained)
1	95.5	1500	0.0004188	0.6282	0.004
2	191	1500	0.0002094	0.3141	-0.007
3	286.47	1500	0.0001396	0.2094	0.263
4	380	1500	0.0001052	0.1579	0.325
5	477.46	1500	0.0000837	0.1256	0.093

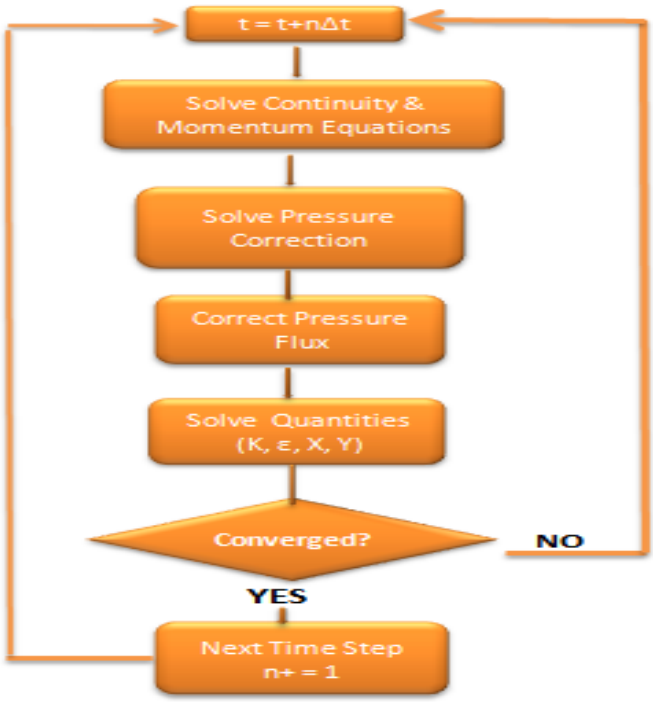

Figure 2.1: Solution strategy in FLUENT (Fluent 12.0.16 user guide).

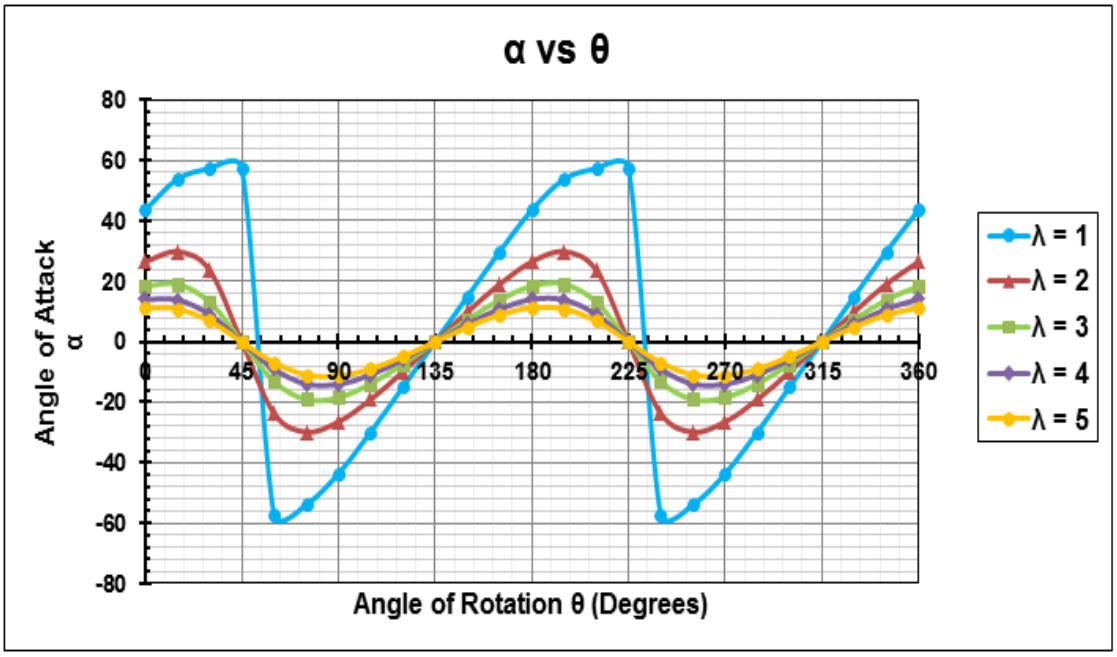

Figure 2.2: Variation of angle of attack as a function of θ in degrees for a range of λ.

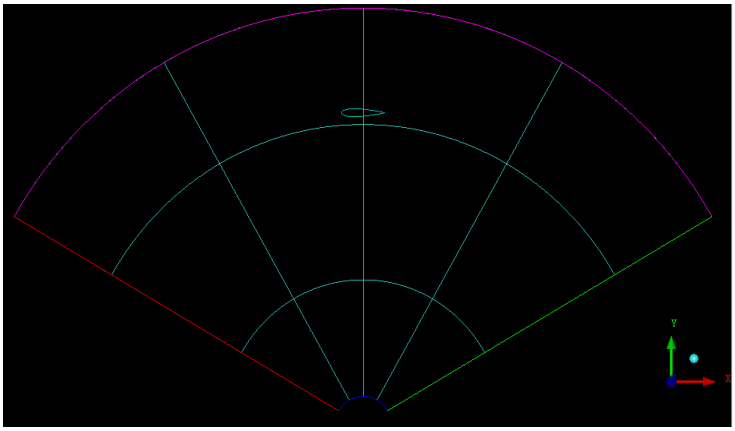

Figure 2.3: Schematic view of the geometry of rotor 120° with NACA 0018 airfoil.

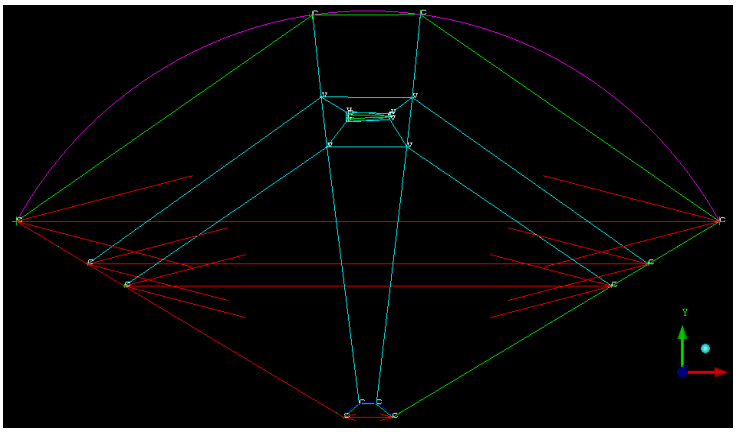

Figure 2.4: Blocking with the application of quarter O-grid and periodic vertices.

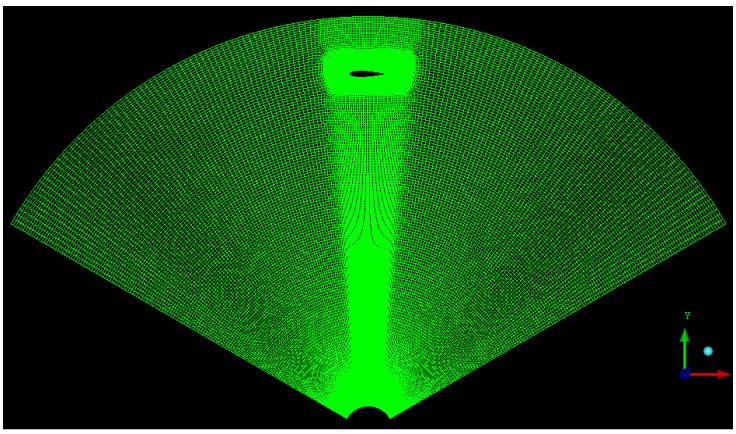

Figure 2.5: Schematic view of the hexahedral meshing of 120° of rotor with NACA0018.

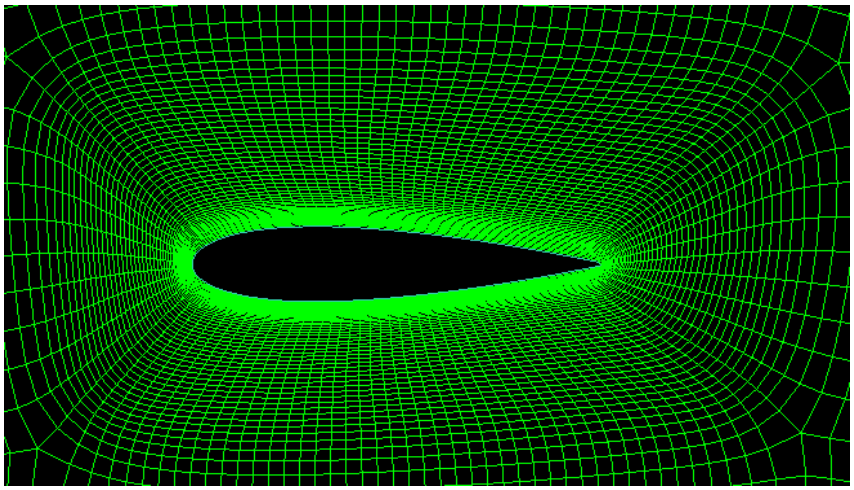

Figure 2.6: Closer view of the O-type grid around NACA0018 airfoil.

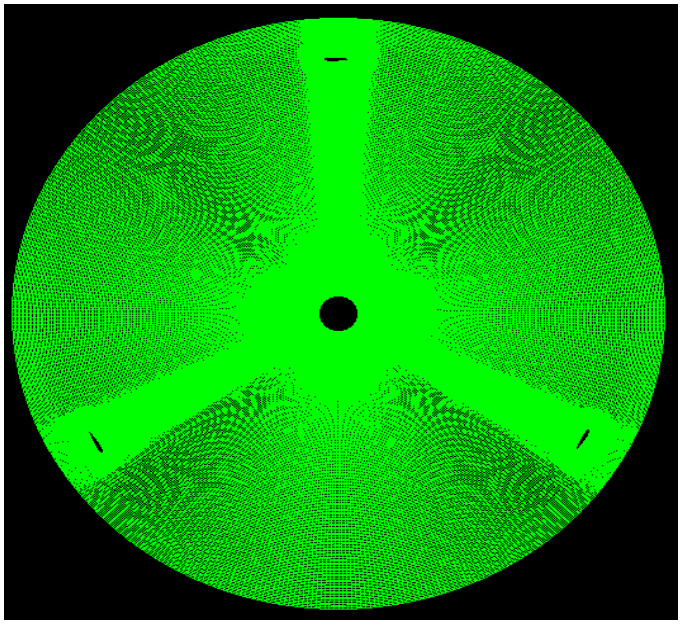

Figure 2.7: View of the rotor (unstructured hexahedral mesh) with three airfoils.

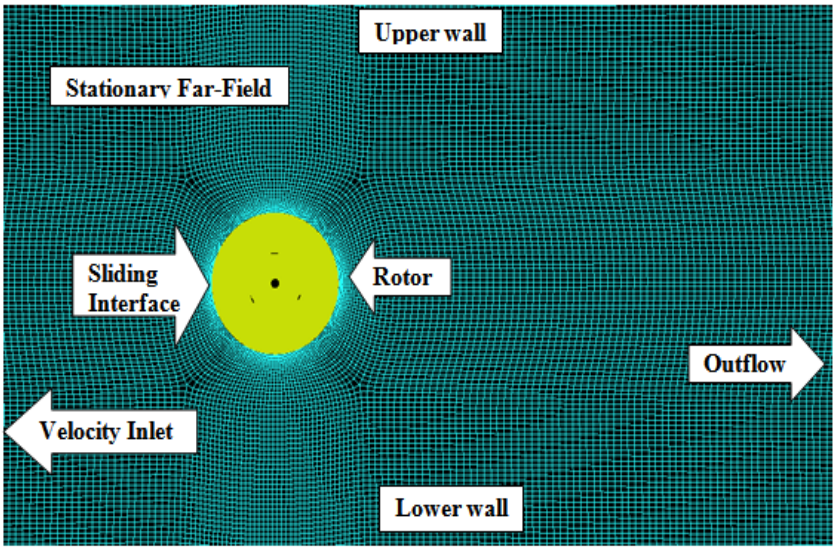

Figure 2.8: Schematic views of the stationary far-field and rotor (unstructured hexahedral mesh).

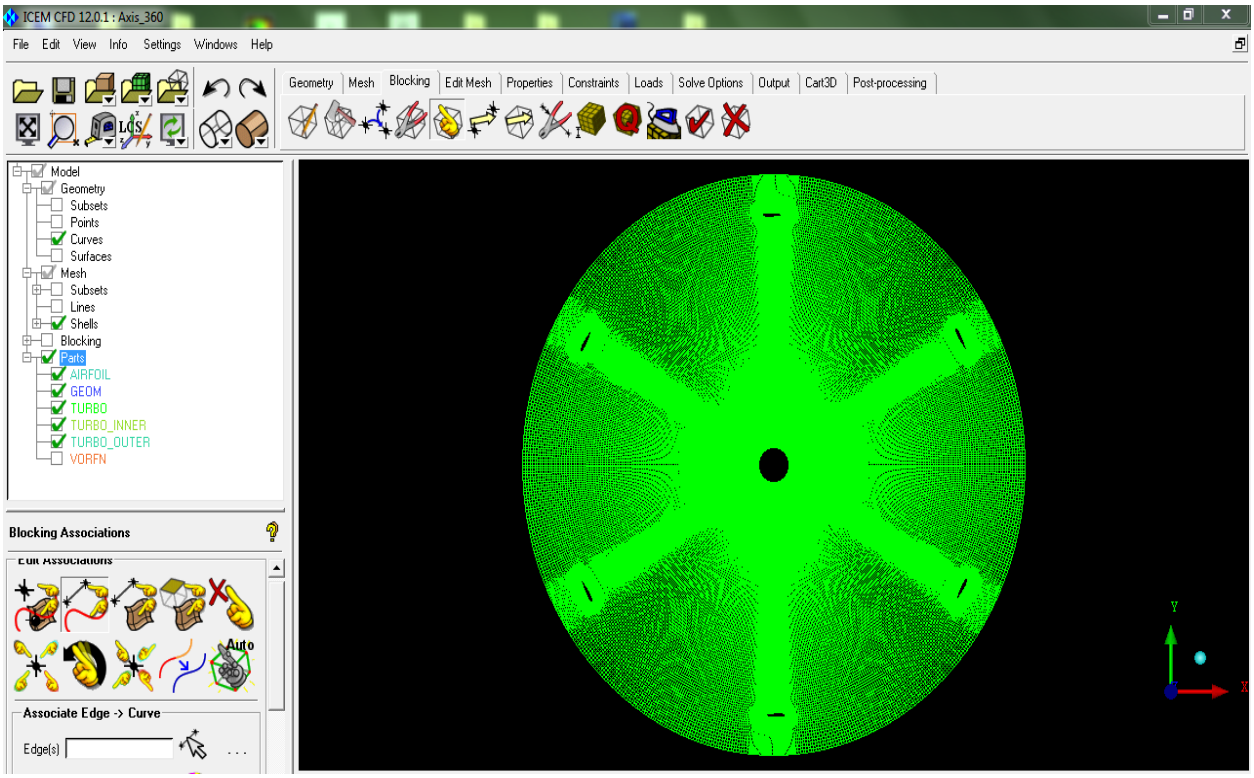

Figure 2.9: Schematic view of a six bladed VAWT with GUI of ICEM CFD.

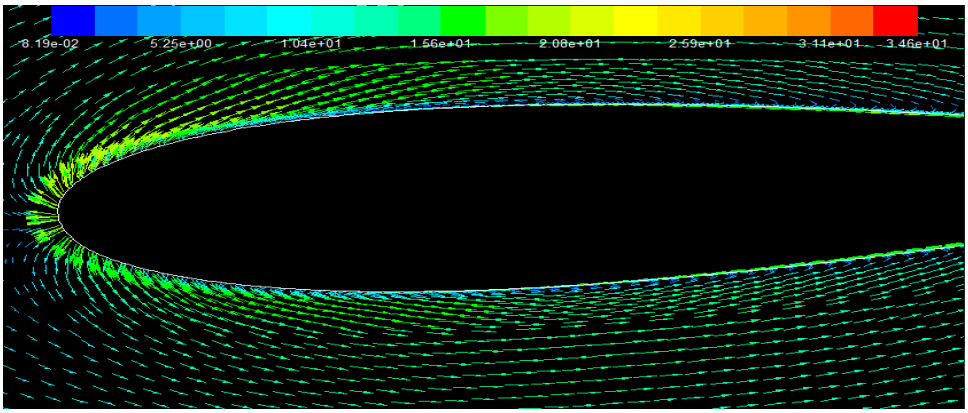

Figure 2.10: Velocity vectors at the surface of the airfoil at $\lambda = 2$, $\theta = 360$, $V_\infty = 10$ m/s, Reynolds number 10^6.

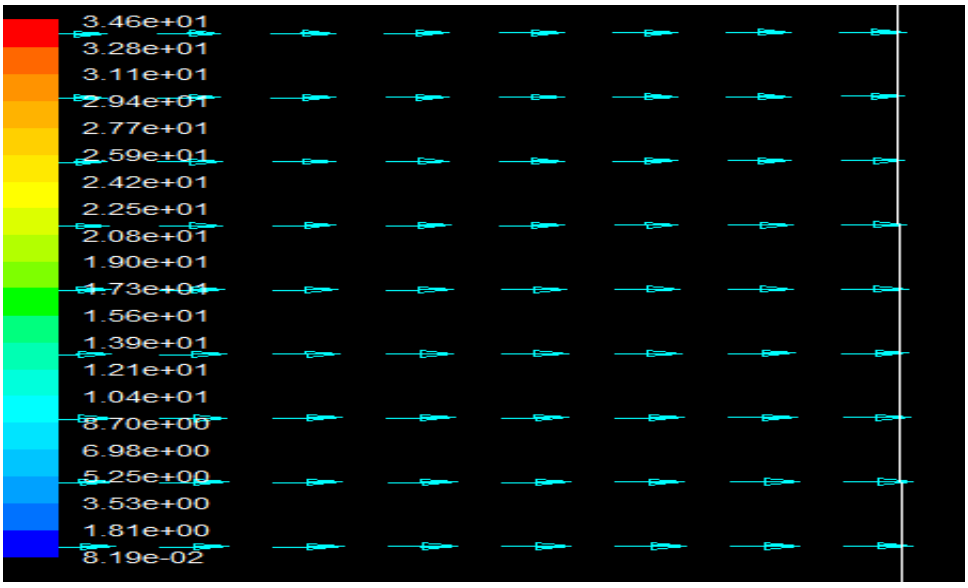

Figure 2.11: Velocity vectors at the outflow at $\lambda = 2$, $V_\infty = 10$ m/s.

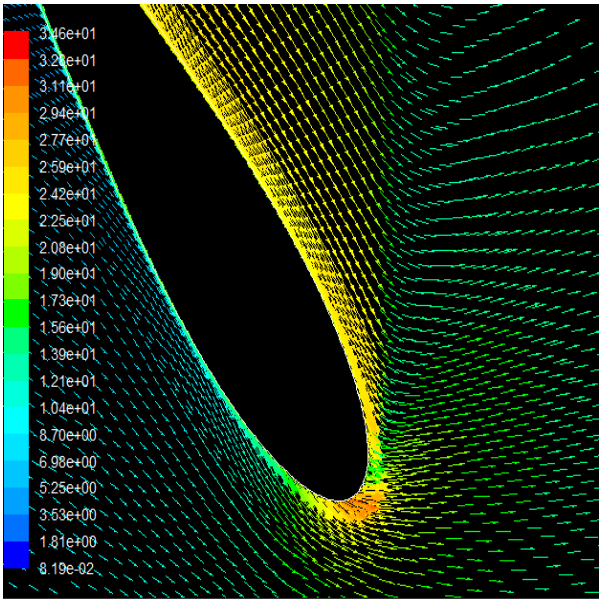

Figure 2.12: Velocity vectors at the leading edge of the airfoil at $\lambda = 2$, $\theta = 120$, V_∞ = 10 m/s.

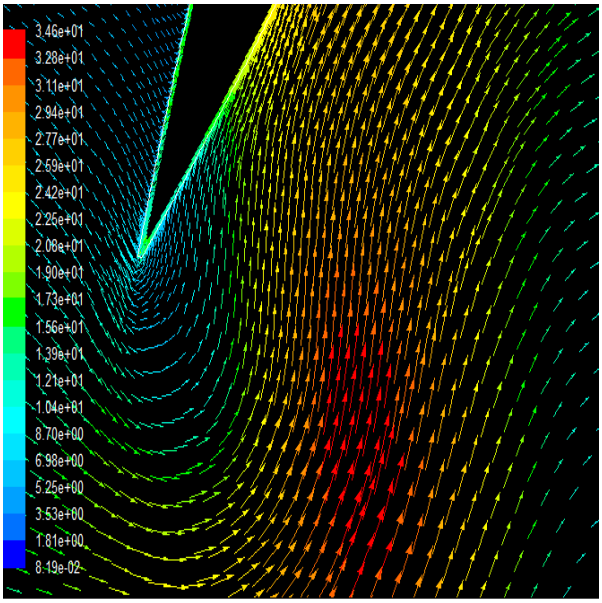

Figure 2.13: Velocity vectors at the trailing edge of the airfoil at $\lambda = 2$, $\theta = 240$, V_∞ = 10 m/s.

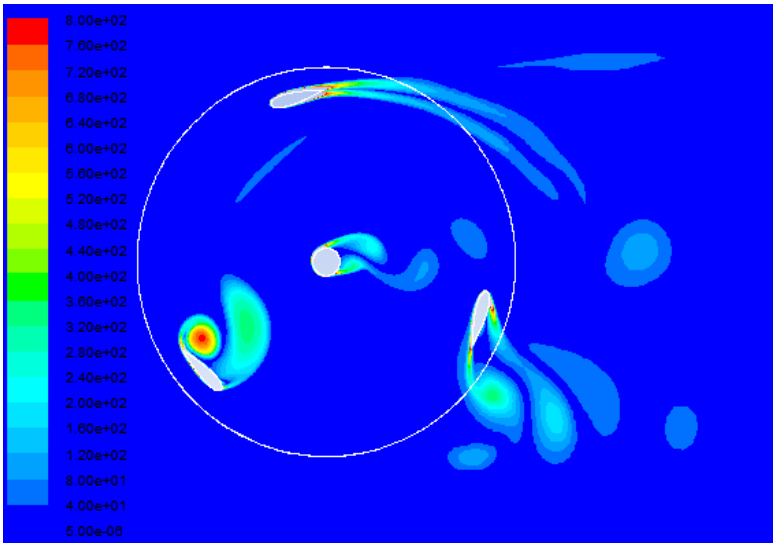

Figure 2.14: Depiction of leading and trailing edge vortex formation

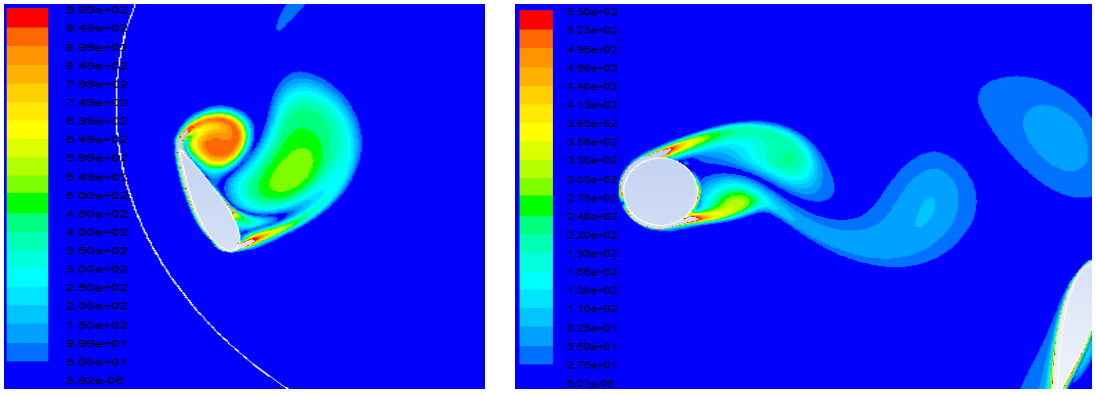

(a) Leading edge vortex and trailing edge vortex.

(b) The tower wake.

Figure 2.15: Formation of vortices at $\lambda = 2$

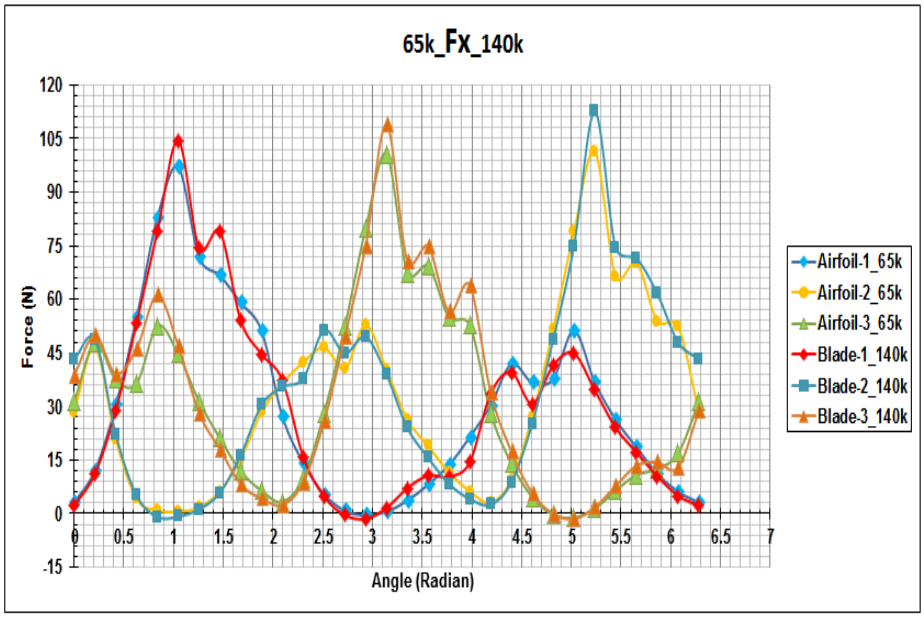

Figure 2.16: Grid-Independent result for cell size of 65000 and 140000 (Horizontal component of the blade force at λ =1.88, V =10 m/s).

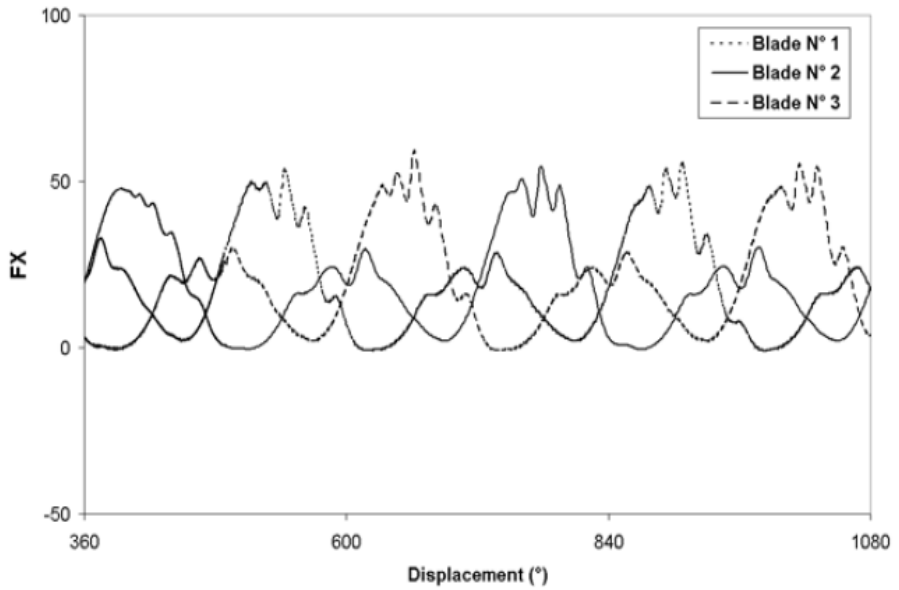

Figure 2.17: Horizontal component of the blade force at λ =1.88, V =10 m/s (Guerri et. al, 2007).

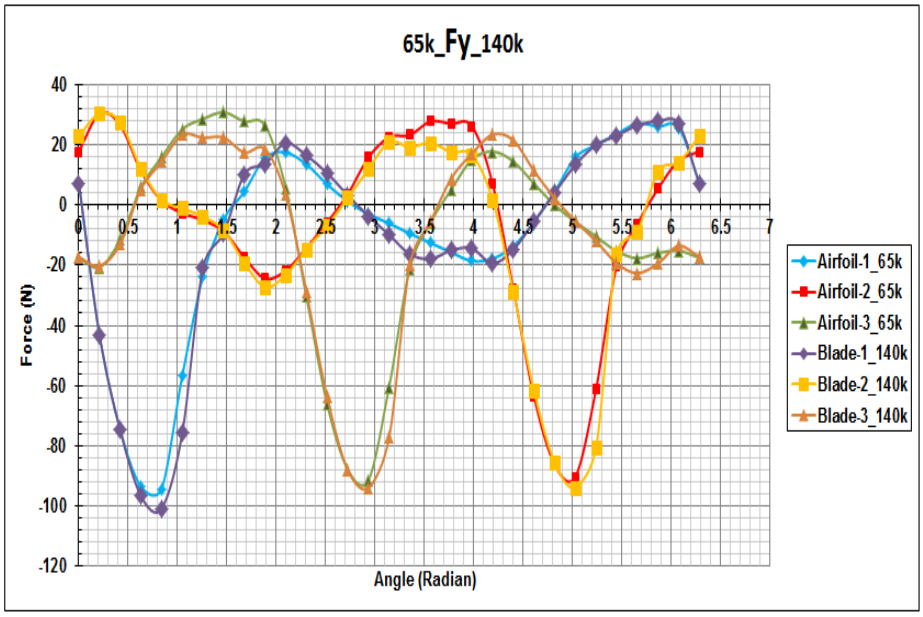

Figure 2.18: Grid-Independent result for cell size of 65000 and 140000 (Vertical component of the blade force at λ =1.88, V =10 m/s).

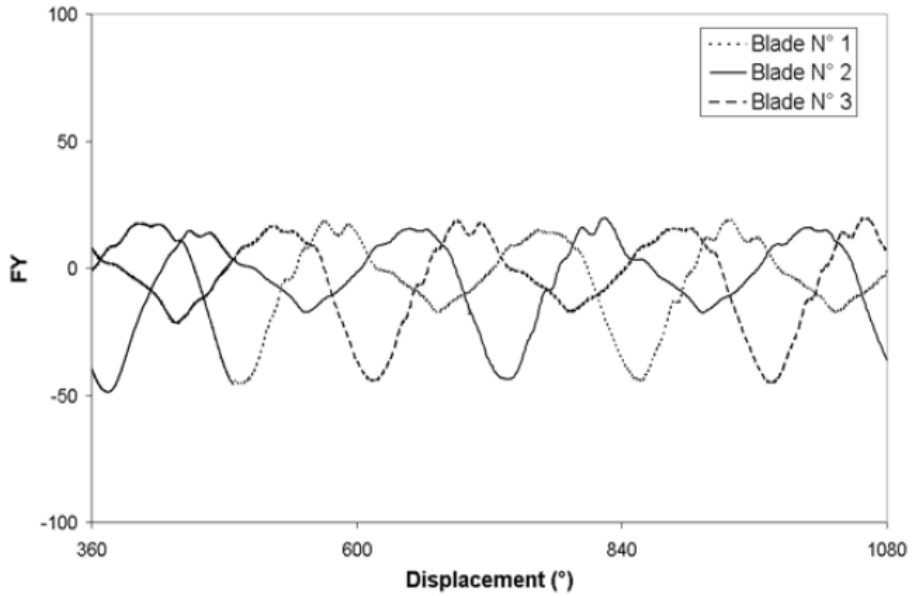

Figure 2.19: Vertical component of the blade force at λ =1.88, V =10 m/s (Guerri et. al, 2007).

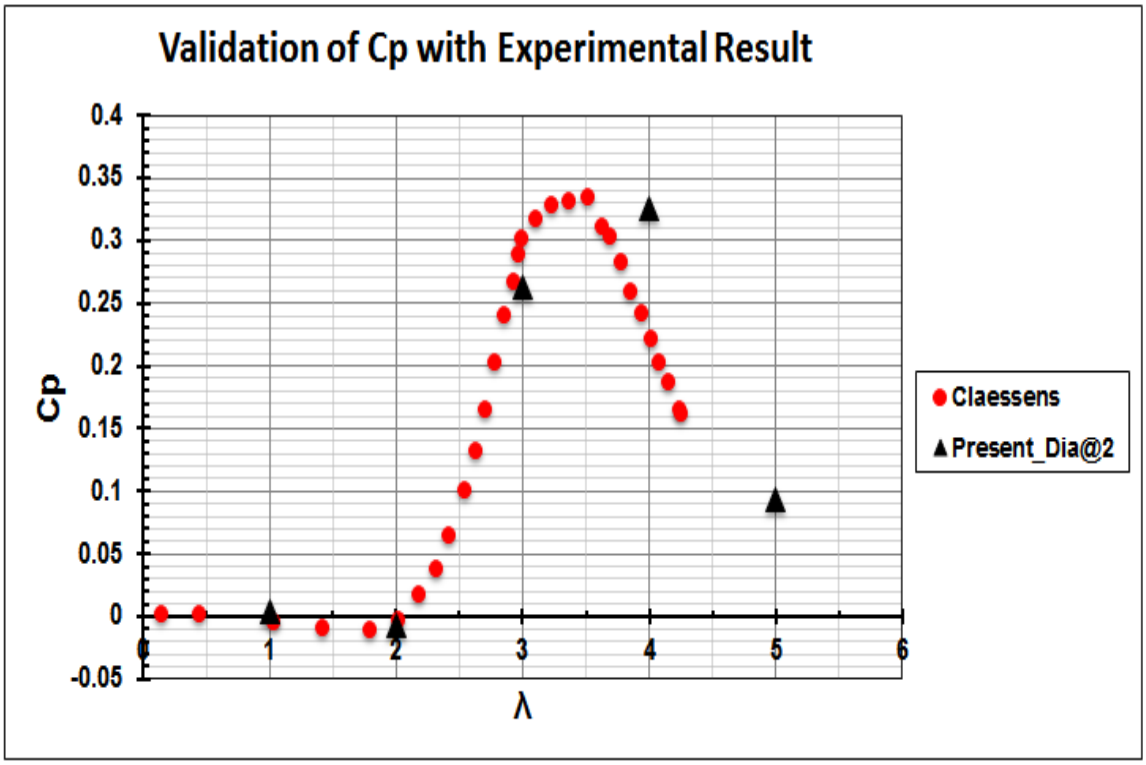

Figure 2.20: (**A**) Validation of C_p of VAWT with the experimental results by Claessens (2006) as a function of λ (**B**) $V_\infty = 10$ m/s, Re $= 10^6$, Rotor diameter= 2 m.

CHAPTER 3

RESULTS AND DISCUSSION

3.1 Introduction

At the lower blade speed the blade torque is expected to be high but the power delivered to the turbine shaft would be low due to the low rotational speed. On the other hand at higher blade speed power would still be low due to the lower torque. Hence, there would be an optimum speed at which turbine would deliver maximum power. Therefore, having a proper ratio between the linear velocity of the tip of the rotor blade and oncoming wind velocity is an important design consideration in order to obtain maximum power output. This ratio is called Tip Speed Ratio. There are several factors that tip speed ratio of the wind turbine depends on such as type and shape of the airfoil used, number of blades, wind velocity and speed of the rotor.

This chapter mainly deals with computational methodology used and results obtained from a proper assessment of an optimum tip speed ratio at which turbine produces maximum power output. Simulation is set to run at several tip speed ratios. Effect of rotor's diameter on turbine's performance is investigated in this chapter. Rotor's diameter is halved (D=1 m.), keeping the wind velocity and tip speed ratio the same as earlier. Result is then analyzed and compared with the results from previous chapter where coefficient of performance of VAWT obtained by CFD simulation was validated with the experimental result by Claessens (2006).

3.2 Coefficient of Performance of a VAWT (C_p)

Coefficient of Performance of a wind turbine is a factor that describes how efficiently wind power is utilized and transformed into useful turbine power. Coefficient of Performance depends on the type of airfoils, blade thickness and Reynolds number. It has been found by experiment that performance increases with the increase in thickness of airfoil. It is basically given by the ratio between power extracted by the turbine and available wind power. It can be mathematically expressed as:-

C_p = Power generated by Turbine/Wind Power

= P_t/P_w

$$C_p = \omega \times T_{mean}/0.5\rho A V^3 \tag{3.1}$$

Average Torque is calculated by reporting coefficient of moment in FLUENT for one complete revolution. It is given by the formula:-

$$T_{mean} = 0.5(\text{Cm1} + \text{Cm2} + \text{Cm3})\rho A V^2 R/\text{number of recorded values} \tag{3.2}$$

Where Cm1, Cm2, Cm3 are coefficient of moments of airfoil-1, airfoil-2 and airfoil-3 respectively.

3.3 Effect of Rotor Diameter on VAWT's Performance

Coefficient of performance is directly proportional to the radius of the rotor. If size of the rotor increases C_p also increases. Following the objective of investigating the effect of turbine size on C_p, rotor's diameter is halved keeping the wind velocity and tip speed ratio the same as earlier. Now in order to maintain the same λ angular velocity of the rotor is doubled and then set up is simulated for a range of λ. Conclusion is drawn by considering the graph between C_p and λ in figure 3.1 that C_p of a wind turbine remains almost same as long as the λ is constant. Fundamentally, the reduction in rotor diameter increases the possibility of blade-blade interaction which

causes more wake generation but in the present case this interaction was not strong enough to cause a decrease in C_p due to the fact that the ratio of chord length and rotor radius (i. e. c/R) were kept the same in both the cases.

3.4 Effect of Laminar Flow on VAWT's Performance By Comparing the Results From RANS Turbulence Model and Laminar Viscous Model

Fluid flow over a body is divided into two categories depending on the relative motion between solid and fluid (White, 2005); one where frictional forces are significant to the flow and another where their effects are negligible. The flow region which is in immediate contact with the body is regarded as a boundary layer. Flow pattern over the airfoil surface goes through several stages from zero velocity at the boundary layer with high friction to maximum velocity away from the boundary layer. Based on the Reynolds number, flow in the boundary layer can be classified as Laminar flow, Transition region flow and Turbulent flow. Reynolds number is the ratio of inertial forces to viscous forces. Flow at low Reynolds number is considered to be a flow where viscous forces are significant whereas flow at high Reynolds number is turbulent due to the dominance of the inertial forces. In the current study both the aspects of fluid flow has been covered. SST k omega model as a RANS Turbulence model is used at Reynolds number of 10^6. Inertial forces at this Reynolds number are too high which causes better aerodynamic performance of NACA 0018 airfoil as compared to low Reynolds number flow. Contours of vorticity at various λ is shown in figure 3.20 and figure 3.21 which illustrates the flow pattern around VAWT at high Reynolds number. Condition of dynamic stall is observed at few angle of attacks and this effect becomes even less significant at high λ. Reynolds number based on chord is given by:

$$Re_c = \frac{\rho V c}{\mu} \tag{3.3}$$

On the other hand, flow around the turbine is also investigated using Laminar

Viscous model at Reynolds number of 5000. As flow velocity over the airfoil surface decreases pressure increases. This causes flow reversal in the boundary layer which leads to flow separation and this separation is called Stall, whereas the bubbles created at leading edge is called leading edge separation bubble. Design of airfoils for low Reynolds numbers are restricted to lift to drag ratio. Symmetrical airfoils like NACA 0018 cannot handle an adverse pressure gradient, causing lower L/D ratio, which eventually leads to flow separation. In order to avoid this problem and maintain a proper lift to drag ratio, usually cambered airfoils are used at low Reynolds numbers. Laminar flow can sustain the pressure gradient to a certain extent after that there may be three possibilities as mentioned by White (2005) (a) complete separation and stall (b) flow separation and then reattachment as turbulent (c) fully turbulent flow. Contours of vorticity at various λ for laminar flow is shown in figure 3.2 and it shows vortices are trailing back due to the flow separation. Wind turbine cannot be conveniently operated below a specific range of Reynolds number as it is obvious from figure 3.3 that turbine produces negative torque at Re = 5000 therefore produces negative power output.

3.5 Effect of Solidity on VAWT's Performance

Optimization of number of blades is really necessary to ensure maximum power output from a wind turbine. If the numbers of rotor blades are less it is supposed to rotate at a much faster rate to sweep out as much wind as possible which may contribute to maximum power output for that configuration. On the other hand if turbine has too many numbers of blades it will obstruct the flow of the wind and will not let sufficient amount of wind to pass through it. Aerodynamic performance, load bearing capacity and total manufacturing cost of the unit are some important factors which must be given a thoughtful consideration while making a choice for the number of blades to be used. Aerodynamic loading is another important factor to be

considered before making a selection of number of blades. In case of Vertical Axis Wind Turbine the blades are not required to be directed towards the wind direction as it is in case of Horizontal Axis Wind turbine. At the same time center of gravity of VAWT lies near the ground as the generator is mounted nearby the ground. Along with having some advantages over HAWT it also possess some disadvantages like when VAWT rotates wind flow produces very high drag force thereby causing a yaw phenomena. This is where alignment of VAWT plays an important role. Cetin et al. (2005) describes an empirical formula to determine the optimum tip speed ratio for a particular number of blades, as follows:-

$$\lambda_{opt} = 4\ \pi/\mathrm{n} \tag{3.4}$$

where n = number of blades. For a 3 bladed wind turbine it should be around 4.18. In the present study $\lambda_{opt} = 3.8$.

Individual torque generated by each blade at several tip speed ratios are shown in figures 3.4 - 3.9 and it shows that torque increases for a range of λ of 2 - 4 and then goes negative due to the generation of dynamic stall. Total torque produced by the turbine at various tip speed ratios are also shown in figures 3.10- 3.15. In order to get an accurate result, simulation is run until steady solution is reached. In most of the cases simulation is found to reach steady state but still in few cases the results are expected to change slightly in the next few cycles. Contours of velocity and contours of pressure of airfoil 1 is shown in figure 3.16 and figure 3.17 at λ = 5 and 3 respectively. In order to make a better comparison of vorticity and wake produced at each λ, for 3 bladed and 6 bladed VAWT, screen-shots of contours of vorticity are attached side by side in figure 3.20 and figure 3.21. Contours of Velocity for 3 bladed and 6 bladed VAWT are also shown in figure 3.18 and figure 3.19. All the contours are clipped to the same range to bring consistency.

Solidity is defined as the ratio of total blade surface area to the area swept by wind turbine blades. Lack of information available regarding the effect of number of blades

on overall performance of a wind turbine gives rise to further the present study in this field. In order to investigate the effect of solidity on C_p, mesh is created for a six bladed VAWT and then CFD simulation is carried out. Simulation is performed at V = 10 m/s, Re = 10^6, D = 2 m. and at values of λ ranging from 1-5. Data sets used for this simulation were kept exactly the same as used earlier for the simulation of 3 bladed wind turbine, just to make a better comparison between their performances. Solidity can be mathematically expressed as follows:

$$\sigma = \frac{N_b C}{R} \tag{3.5}$$

Where:

N_b = Total number of blades (6 for the present case)

C = Blade chord length

R = Rotor radius

It is concluded from the CFD results that blockage effect increases with the increase in number of blades which causes low entrance velocity and leads to higher torque generation. This effect is more significant at higher values of λ. Another conclusion that can be drawn from the result is, the corresponding value of λ for $C_{p,max}$ of wind turbine decreases with the increase in number of blades or in other words maximum C_p is obtained at relatively lower value of λ as the number of blades increases. It is obvious from the figure 3.22 that $C_{p,max} = 0.34$ is achieved at $\lambda = 3.8$ for 3 bladed VAWT whereas for 6 bladed VAWT $C_{p,max} = 0.39$ is achieved at $\lambda = 2.8$. A conclusion can be drawn from figure 3.20 and 3.21 that for 6 bladed turbine wake interaction between blades take place more frequently as compared to 3 bladed turbine which means that $C_{p,max}$ could be obtained at relatively lower value of λ as compared to 3 bladed VAWT.

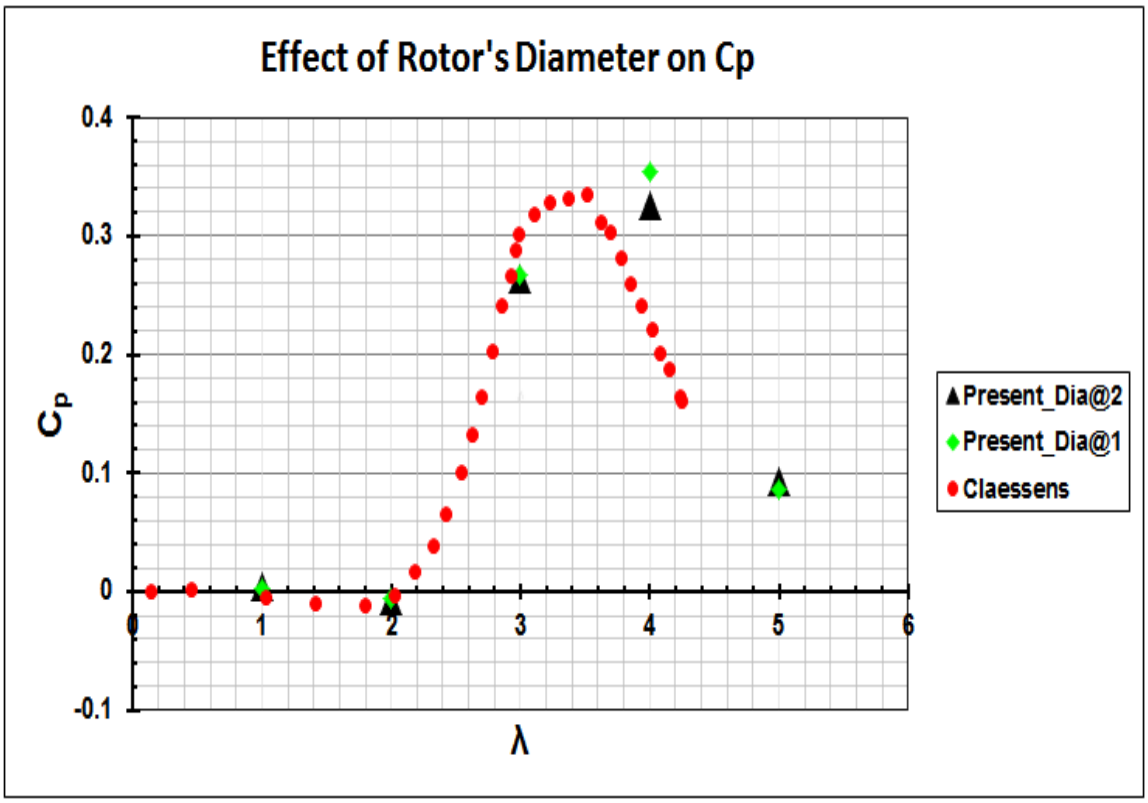

Figure 3.1: (**A**) Influence of rotor diameter on the VAWT's performance for a range of λ (**B**) $V_\infty = 10$ m/s, Re $= 10^6$, Rotor diameter 1m. and 2m.

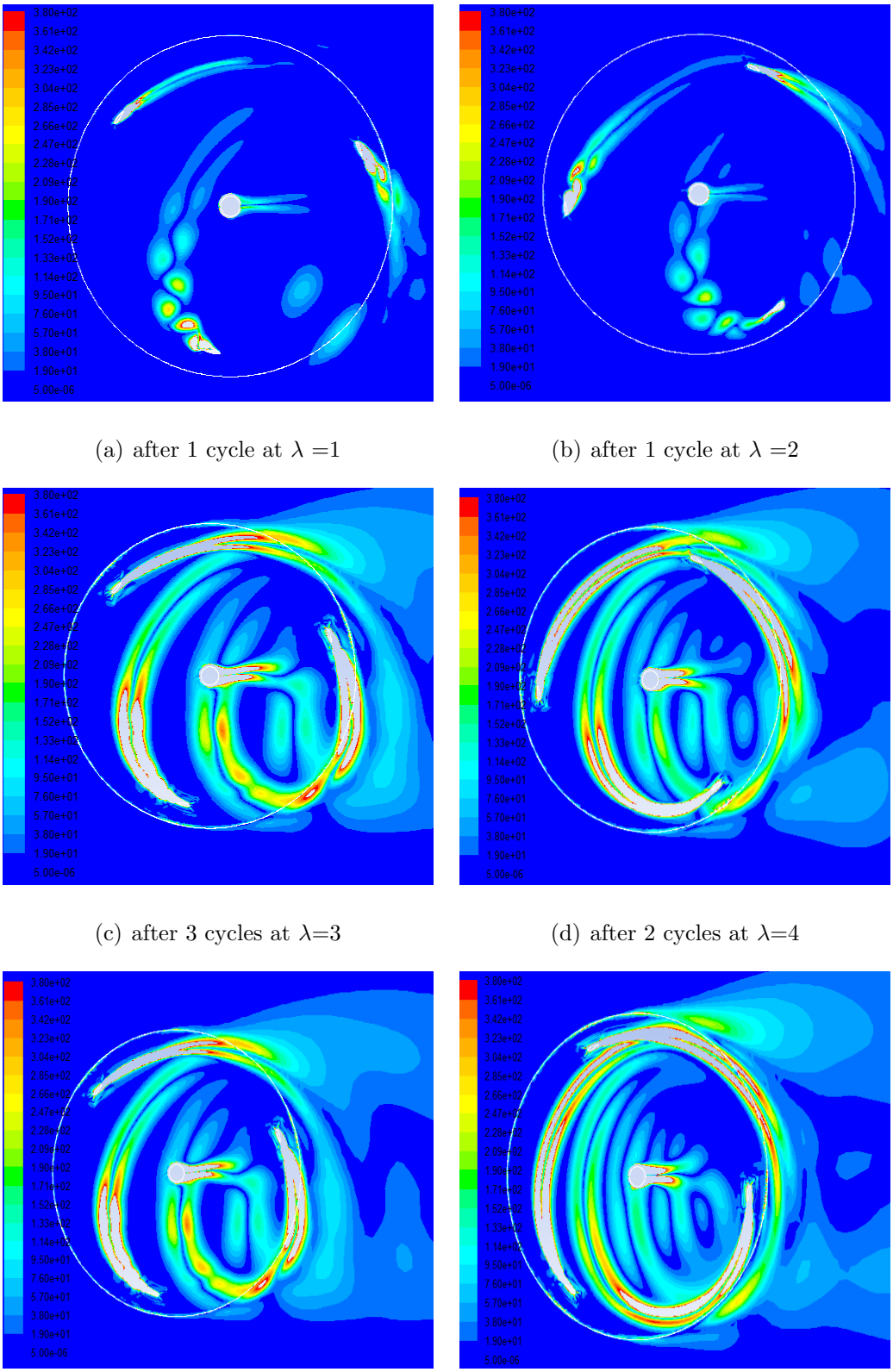

(a) after 1 cycle at λ =1

(b) after 1 cycle at λ =2

(c) after 3 cycles at λ=3

(d) after 2 cycles at λ=4

(e) after 2 cycles at λ=5

(f) after 3 cycles at λ=6

Figure 3.2: Contours of Vorticity for a range of λ for Laminar flow at Re_c =5000, D = 0.1365 m.

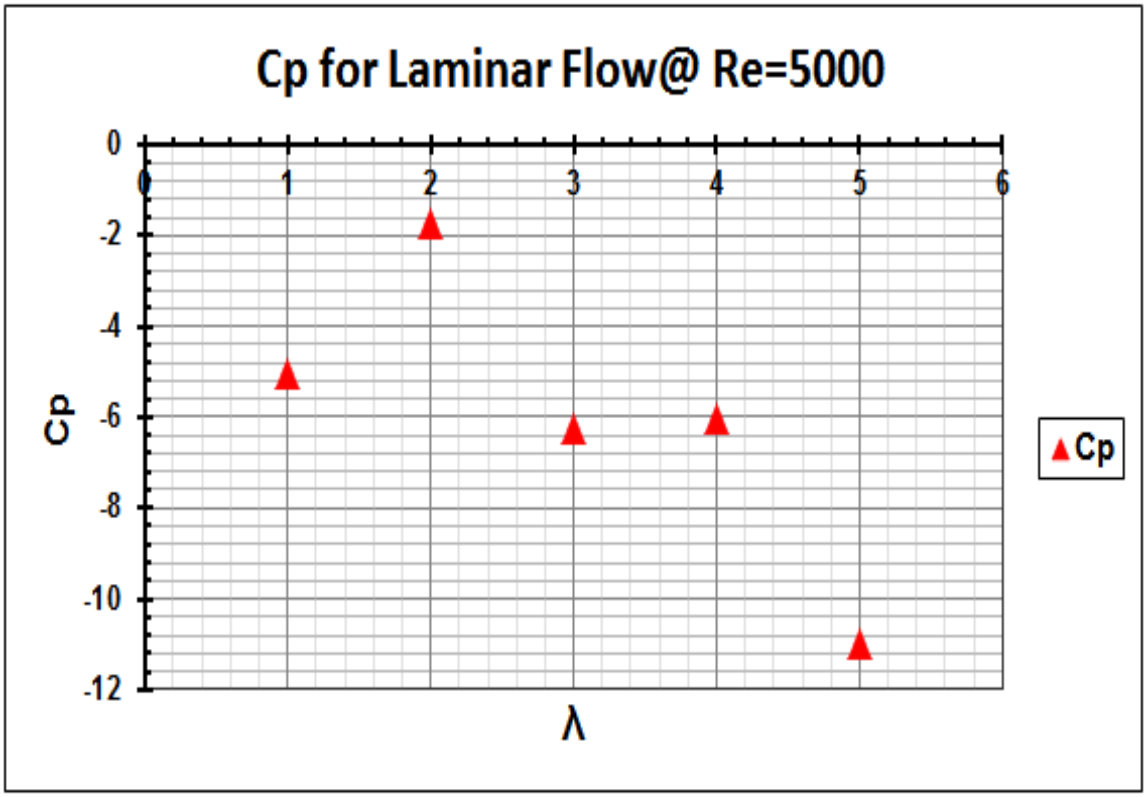

Figure 3.3: Influence of Laminar flow on C_p with the application of Laminar viscous model at low Re_c= 5000, V_∞ = 10 m/s, Rotor diameter= 0.1365 m.

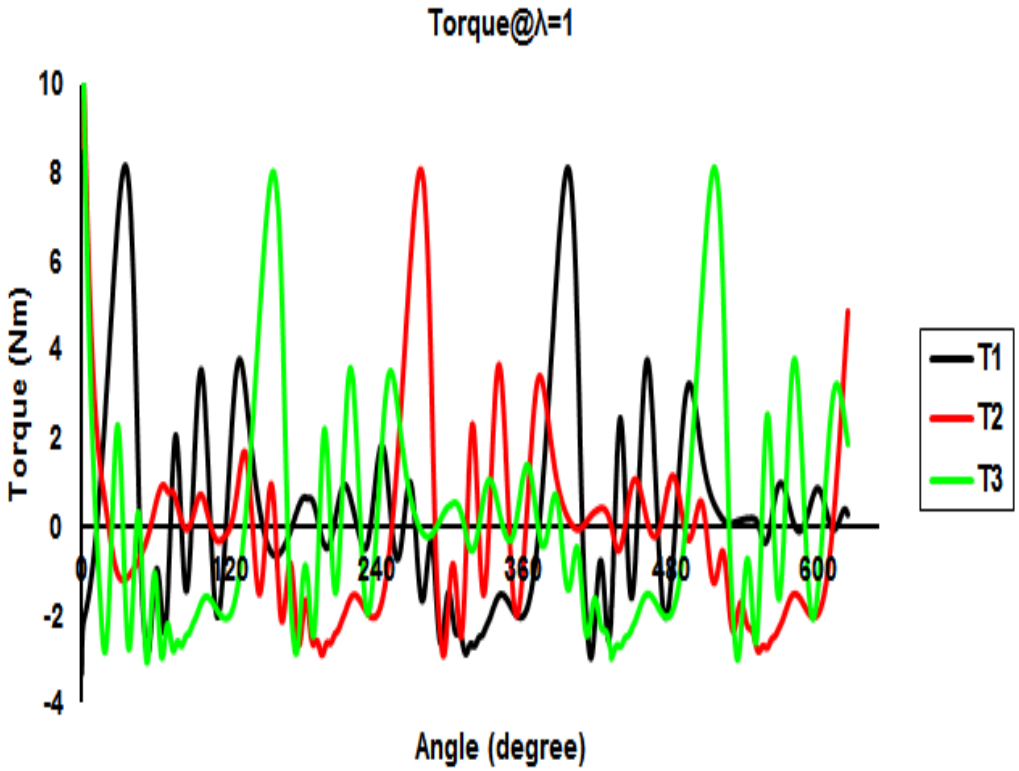

Figure 3.4: Variation of torque generated by each blade as a function of $\lambda = 1$

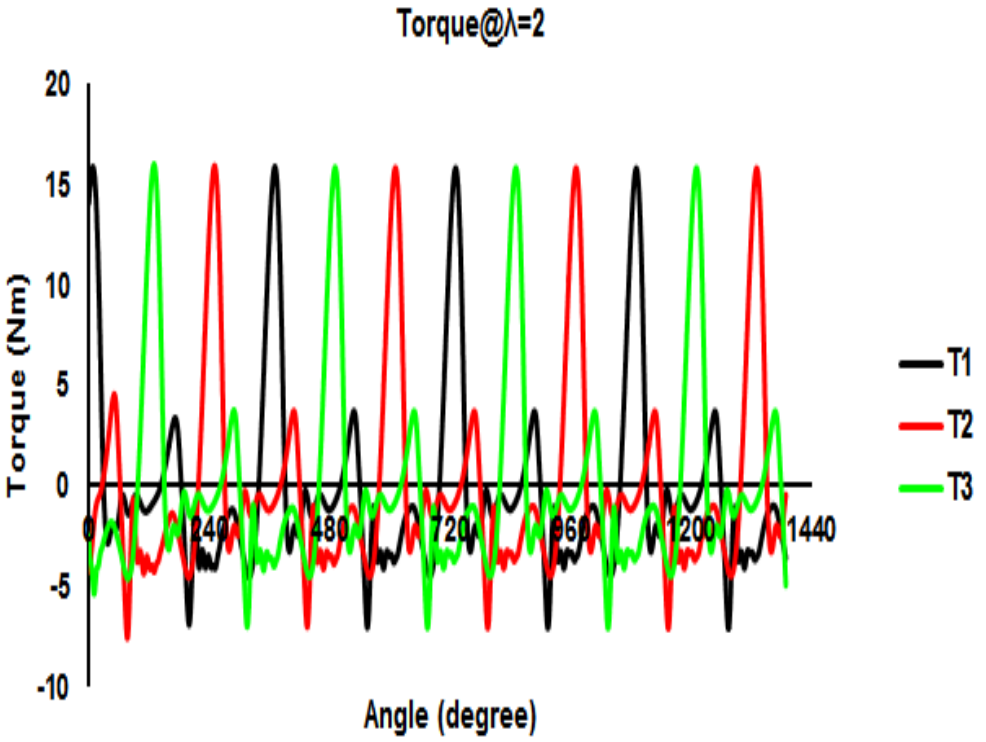

Figure 3.5: Variation of torque generated by each blade as a function of $\lambda = 2$

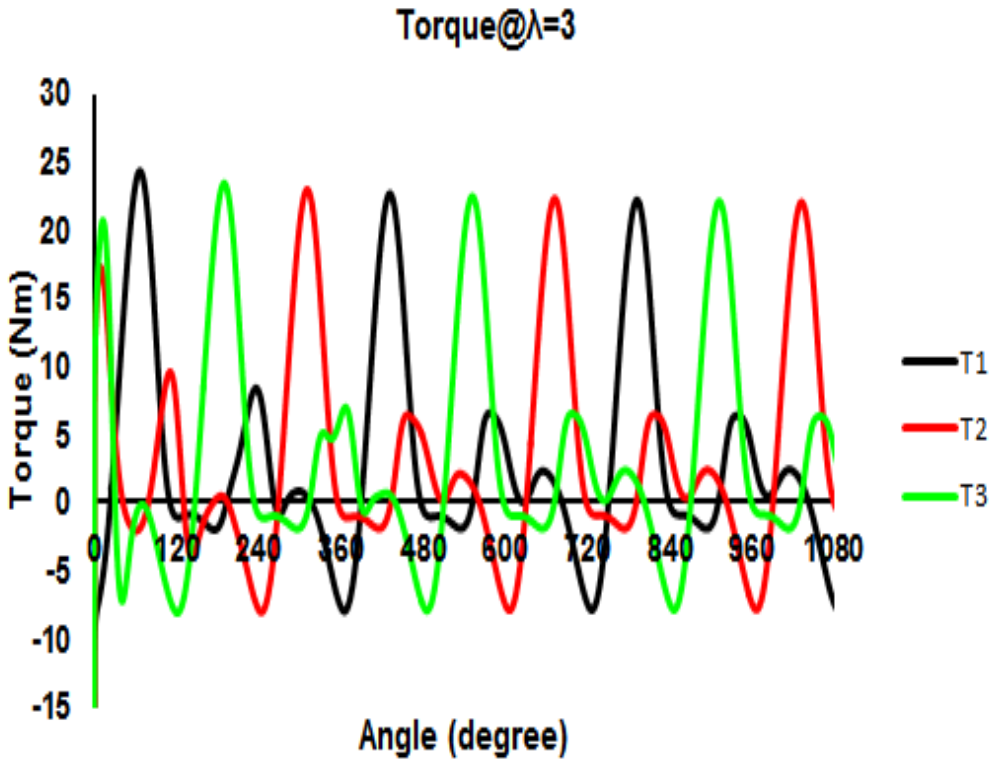

Figure 3.6: Variation of torque generated by each blade as a function of $\lambda = 3$

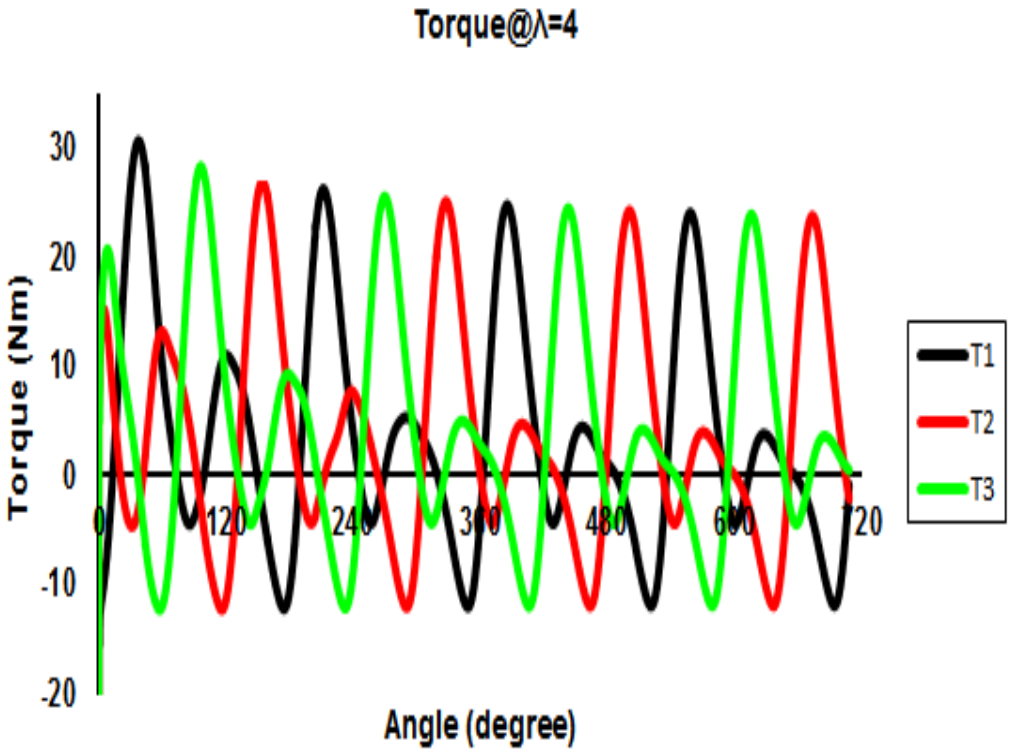

Figure 3.7: Variation of torque generated by each blade as a function of $\lambda = 4$

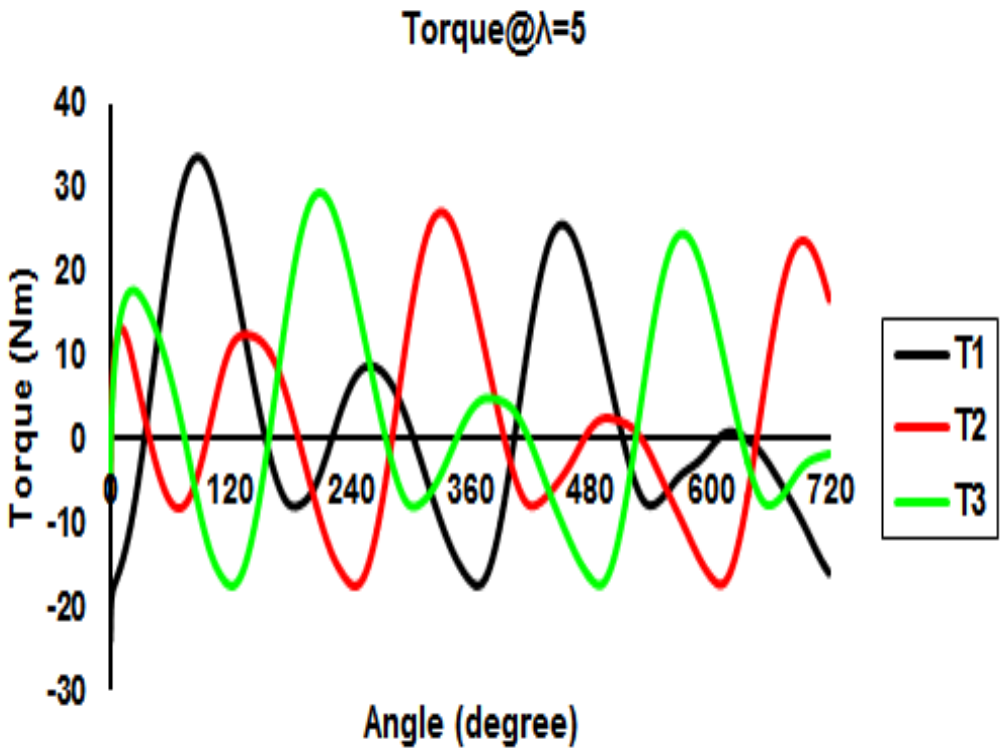

Figure 3.8: Variation of torque generated by each blade as a function of $\lambda = 5$

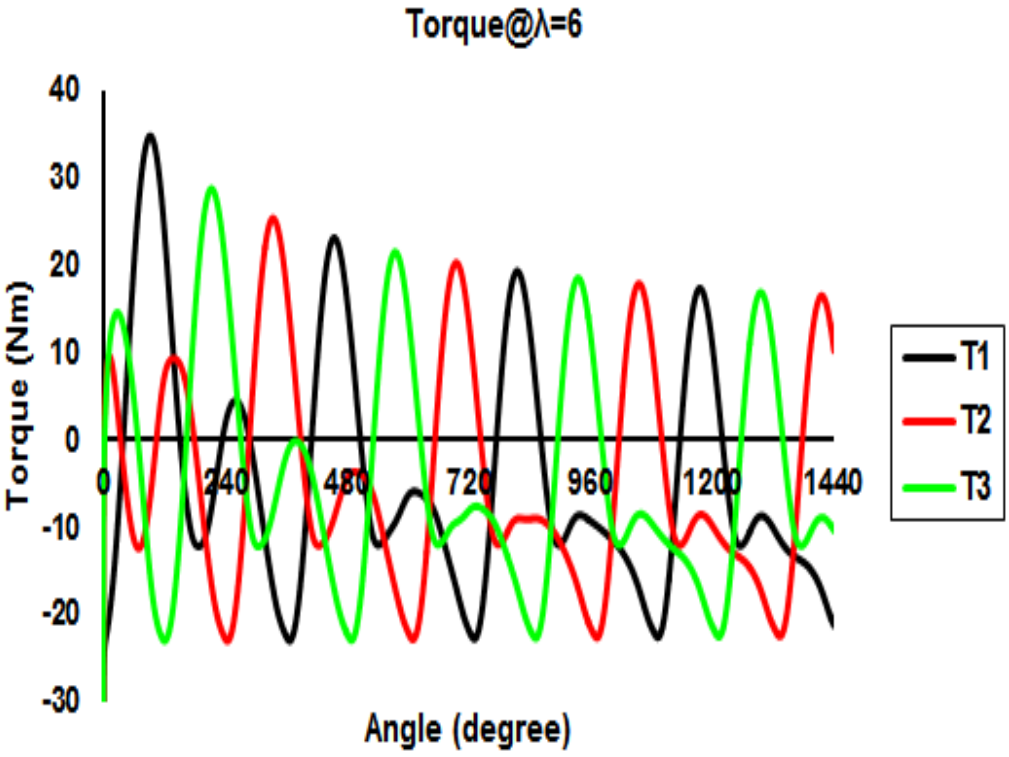

Figure 3.9: Variation of torque generated by each blade as a function of $\lambda = 6$

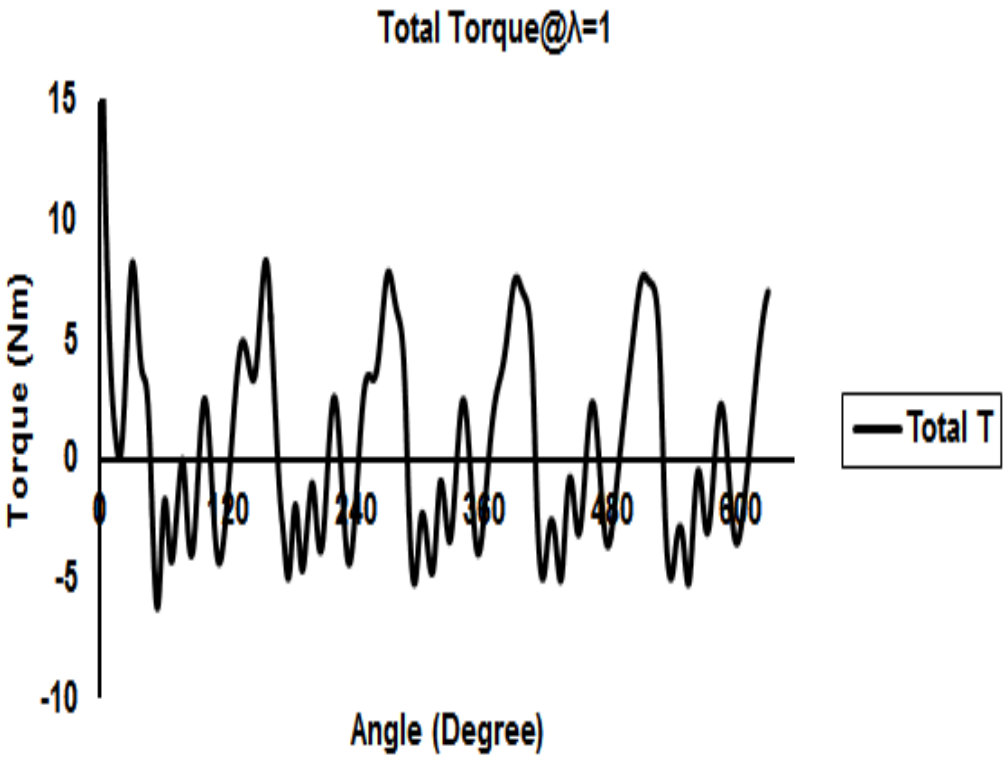

Figure 3.10: Variation of total torque generated by VAWT as a function of $\lambda = 1$

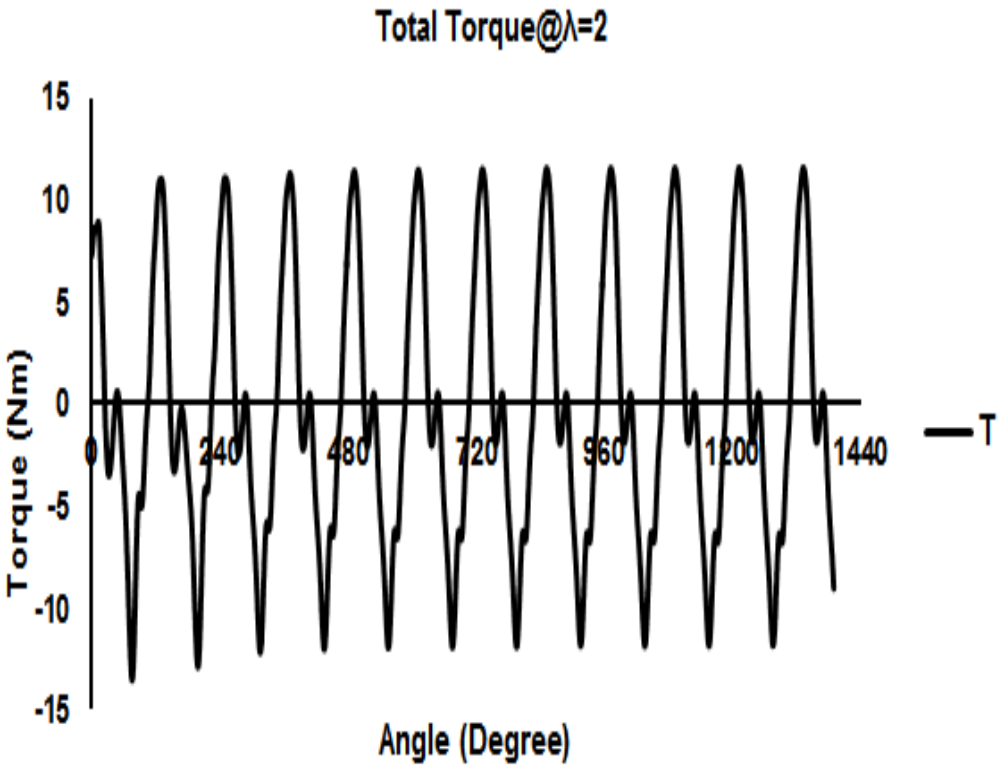

Figure 3.11: Variation of total torque generated by VAWT as a function of $\lambda = 2$

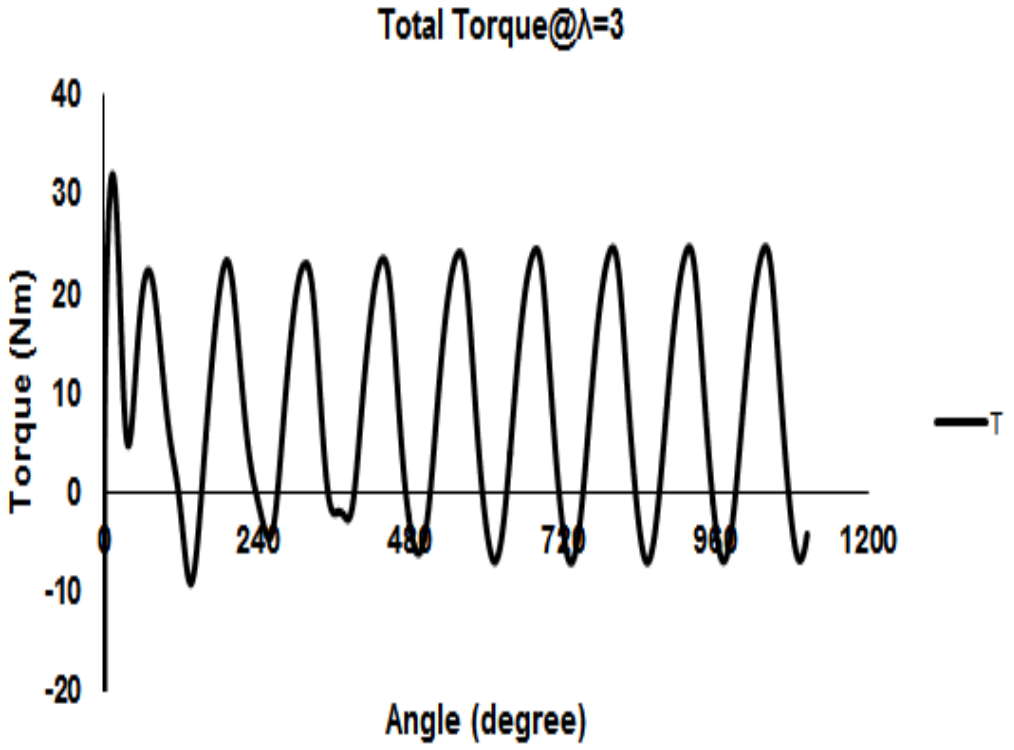

Figure 3.12: Variation of total torque generated by VAWT as a function of $\lambda = 3$

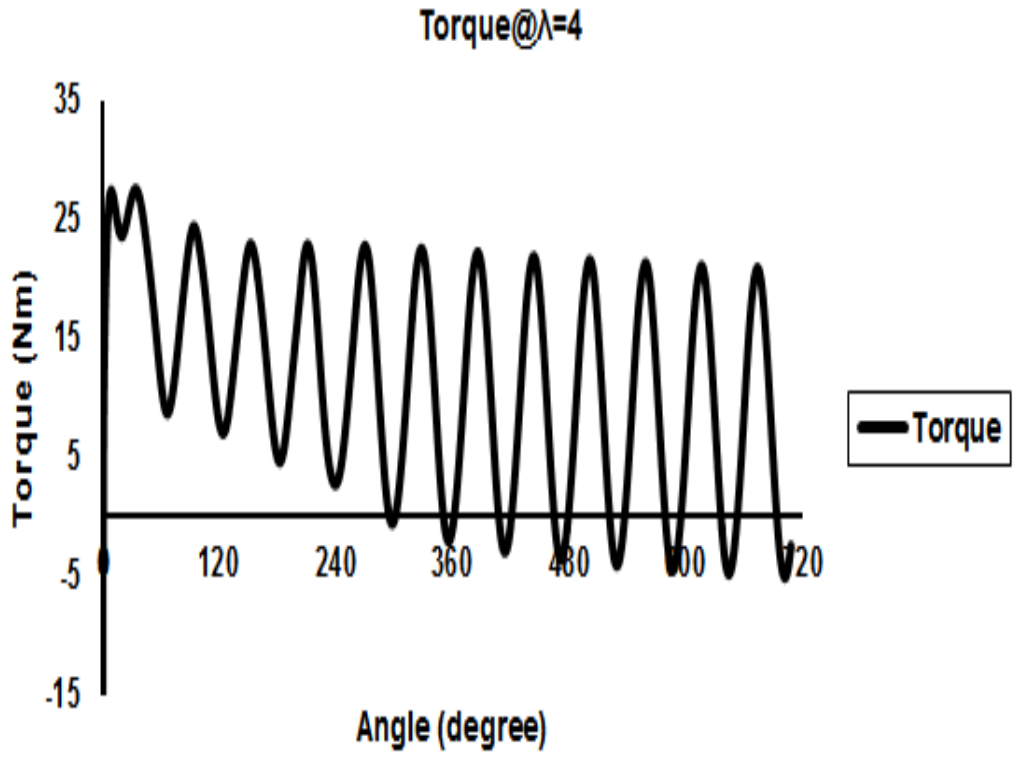

Figure 3.13: Variation of total torque generated by VAWT as a function of $\lambda = 4$

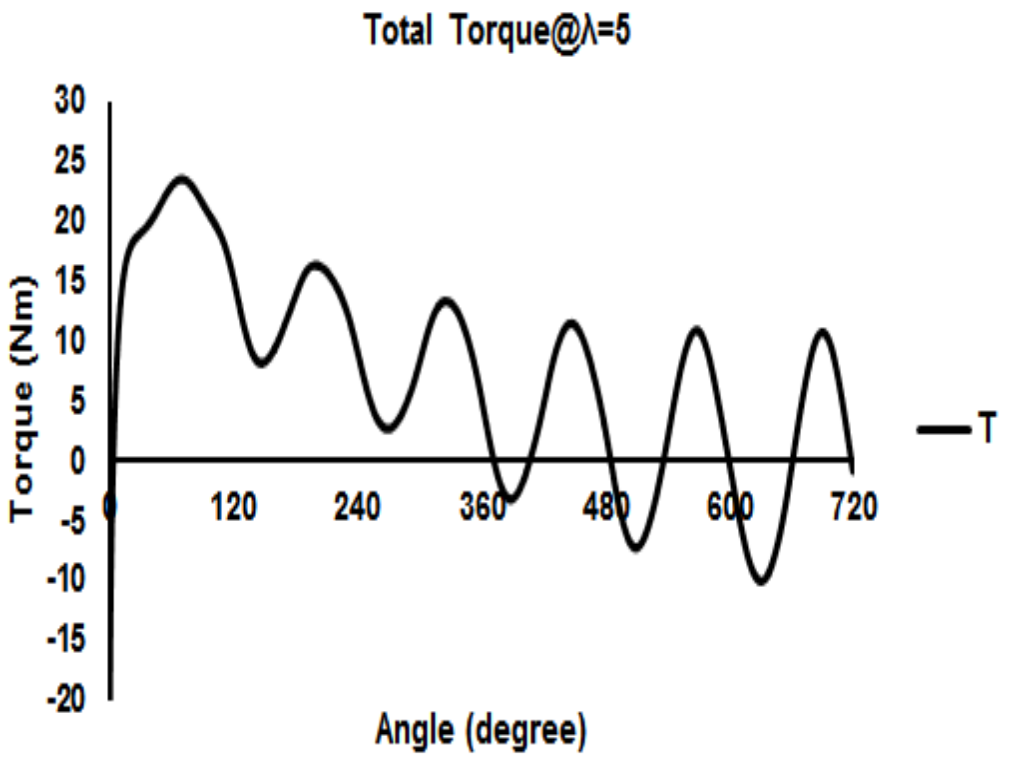

Figure 3.14: Variation of total torque generated by VAWT as a function of $\lambda = 5$

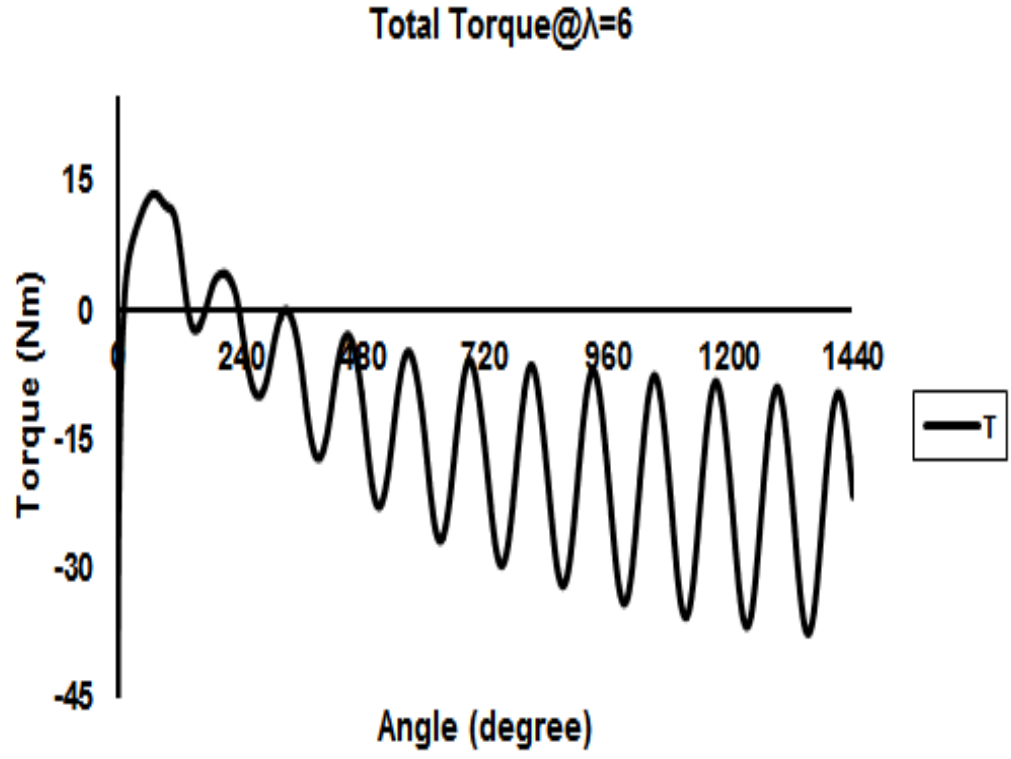

Figure 3.15: Variation of total torque generated by VAWT as a function of $\lambda = 6$

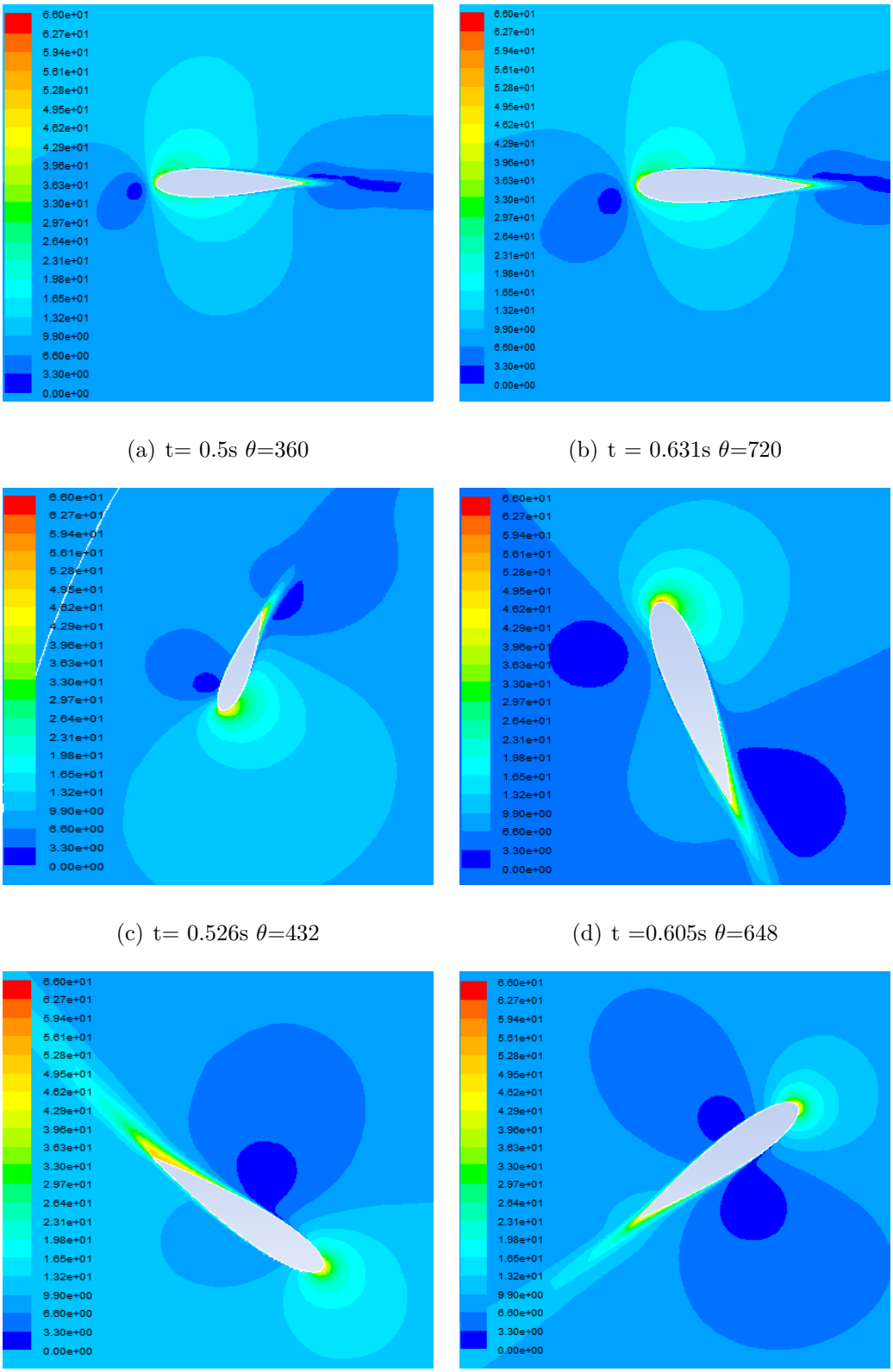

(a) t= 0.5s θ=360

(b) t = 0.631s θ=720

(c) t= 0.526s θ=432

(d) t =0.605s θ=648

(e) t= 0.552s θ=504

(f) t= 0.578s θ=576

Figure 3.16: Contours of Velocity of airfoil-1 after two cycles at λ =5 and $Re_c = 10^6$

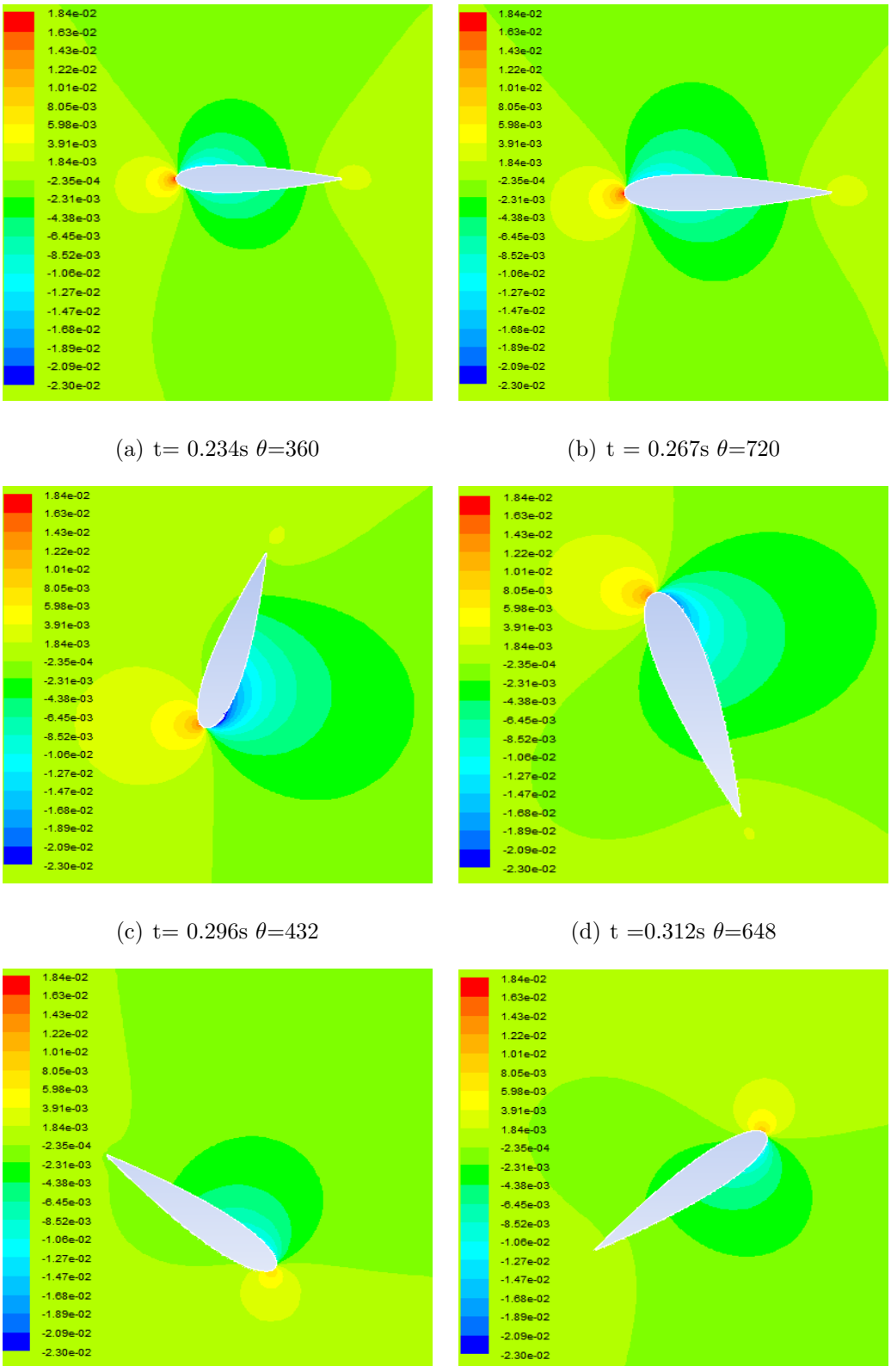

(a) t= 0.234s θ=360

(b) t = 0.267s θ=720

(c) t= 0.296s θ=432

(d) t =0.312s θ=648

(e) t= 0.362s θ=504

(f) t= 0.413s θ=576

Figure 3.17: Contours of Pressure of airfoil-1 after two cycles at λ =3 and $Re_c = 10^6$

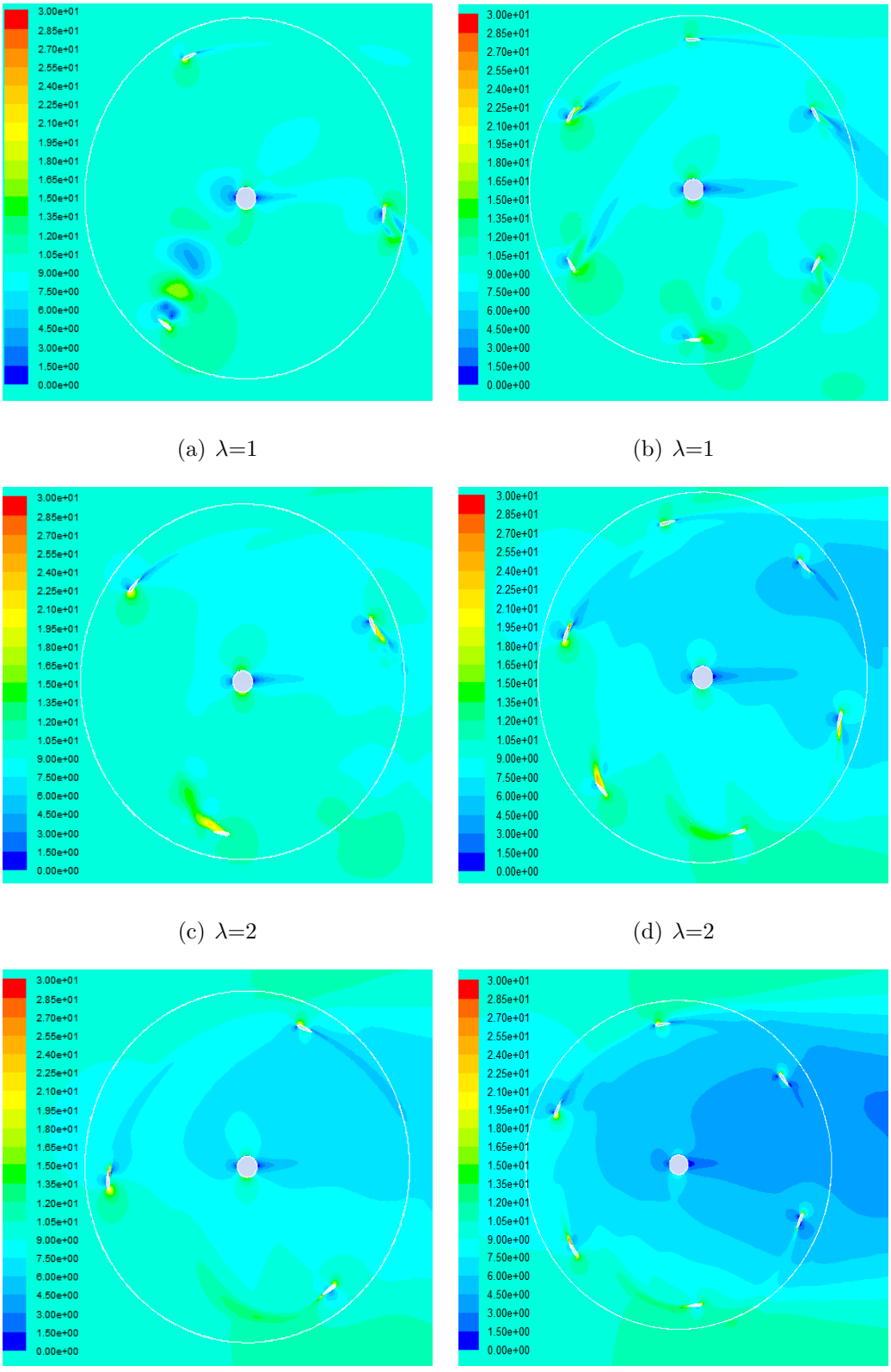

(a) λ=1 (b) λ=1

(c) λ=2 (d) λ=2

(e) λ=3 (f) λ=3

Figure 3.18: Contours of Velocity at $\lambda = 1, 2, 3$ and $Re_c = 10^6$, for 3 bladed turbine on left side and 6 bladed turbine on right side

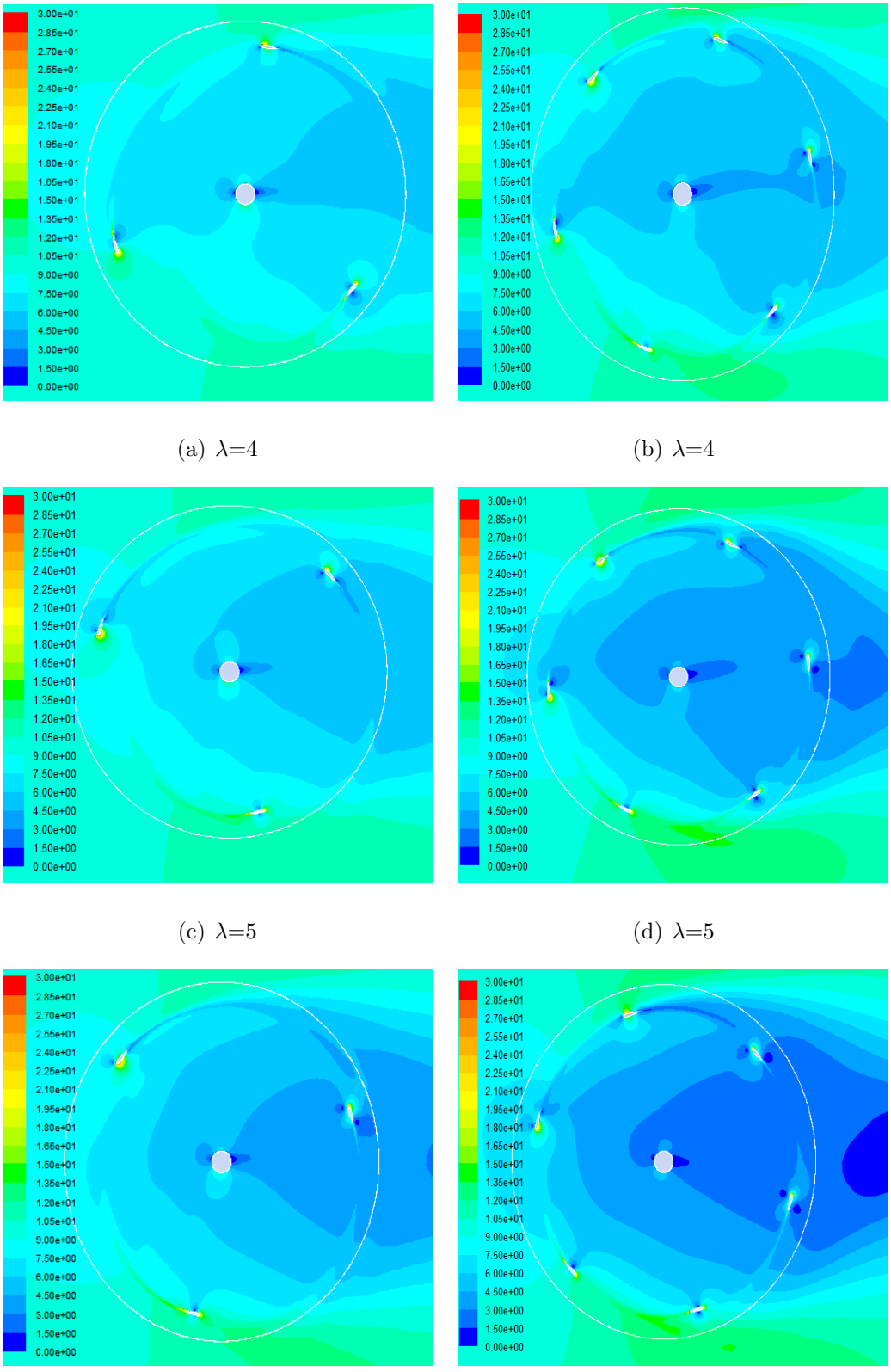

(a) λ=4 (b) λ=4

(c) λ=5 (d) λ=5

(e) λ=6 (f) λ=6

Figure 3.19: Contours of Velocity at $\lambda = 4, 5, 6$ and $Re_c = 10^6$, for 3 bladed turbine on left side and 6 bladed turbine on right side

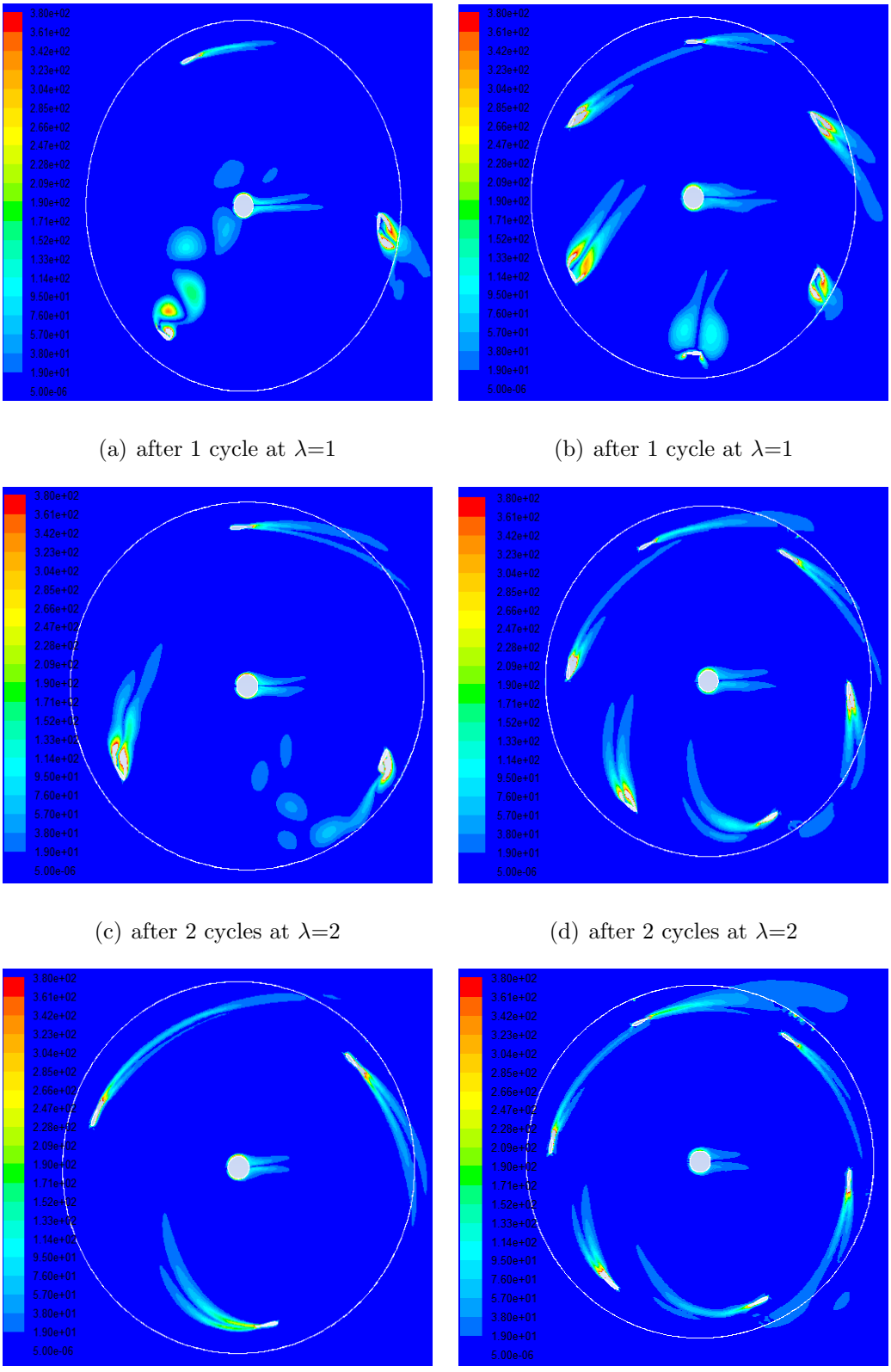

(a) after 1 cycle at λ=1

(b) after 1 cycle at λ=1

(c) after 2 cycles at λ=2

(d) after 2 cycles at λ=2

(e) after 2 cycles at λ=3

(f) after 2 cycles at λ=3

Figure 3.20: Contours of Vorticity at $\lambda = 1$, 2, 3 and $Re_c = 10^6$, for 3 bladed turbine on left side and 6 bladed turbine on right side

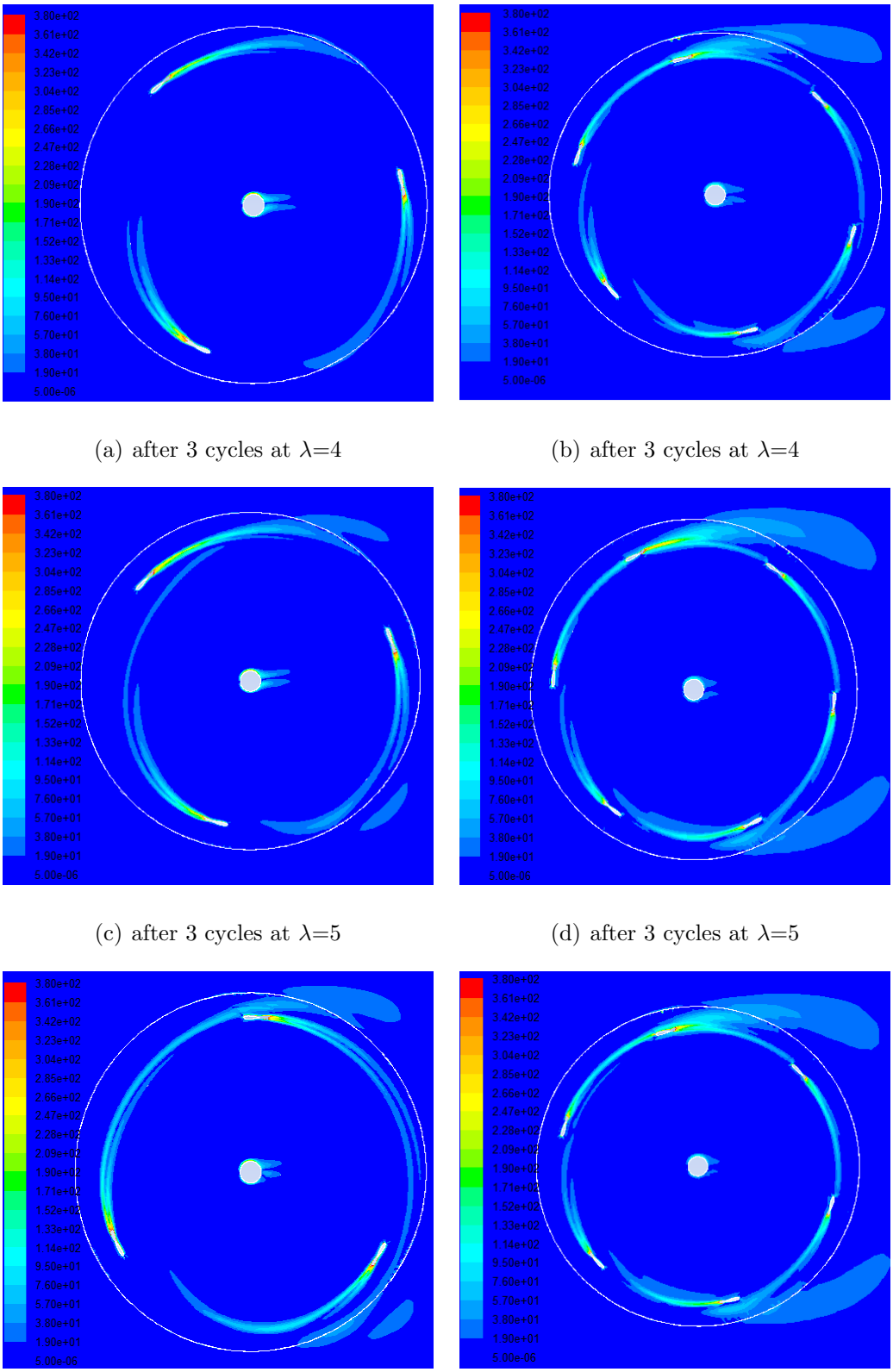

(a) after 3 cycles at λ=4

(b) after 3 cycles at λ=4

(c) after 3 cycles at λ=5

(d) after 3 cycles at λ=5

(e) after 2 cycles at λ=6

(f) after 2 cycles at λ=6

Figure 3.21: Contours of Vorticity at $\lambda = 4$, 5, 6 and $Re_c = 10^6$, for 3 bladed turbine on left side and 6 bladed turbine on right side

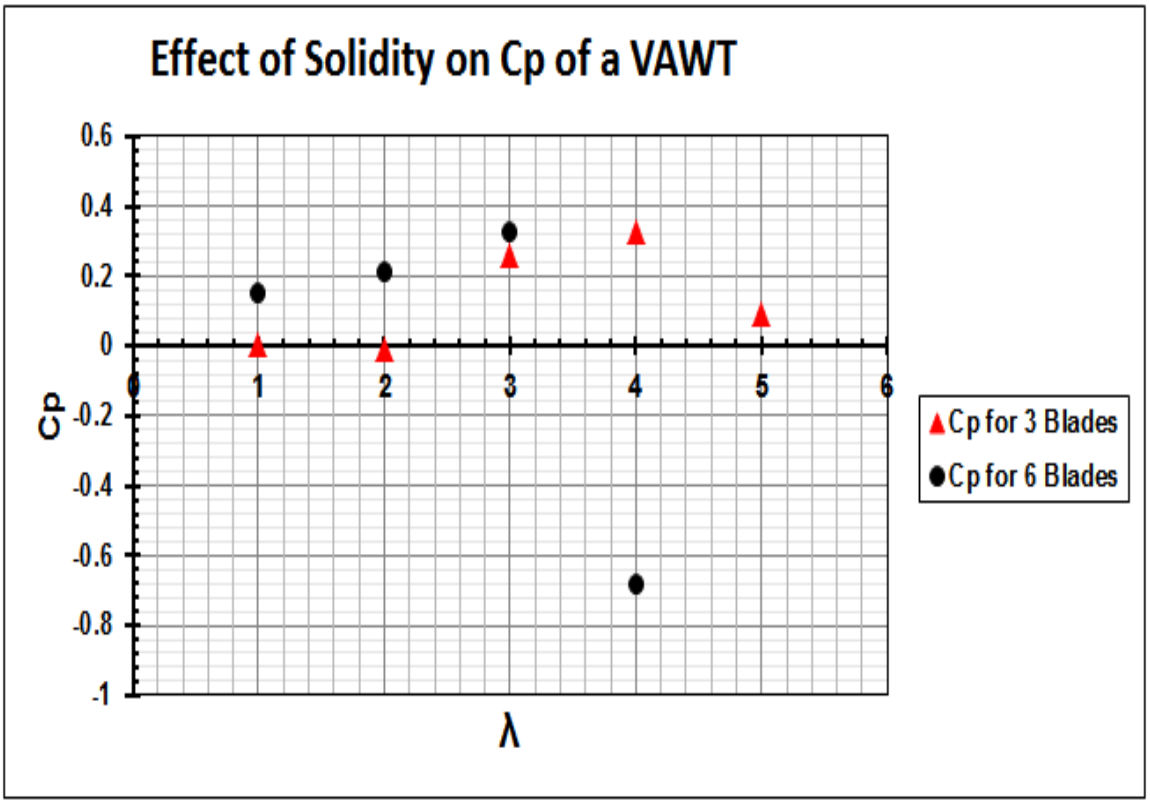

Figure 3.22: (**A**) Influence of number of blades on the VAWT's performance for a range of λ (**B**) V_∞ = 10 m/s, Re = 10^6, Rotor diameter= 2 m.

Table 3.1: Data sets used for simulation in FLUENT (V_∞ = 10 m/s, Rotor Diameter = 1 m.)

TSR	Speed in RPM	Total Time Steps	Step Size δt	Total Time/cycle	Cp(obtained)
1	191	1500	0.0002094	0.3141	0.00271
2	382	1500	0.0001047	0.1570	-0.0054
3	572.94	1500	0.0000698	0.1047	0.267
4	760	1500	0.00005263	0.0789	0.354
5	954.92	1500	0.00004188	0.0628	0.087

Table 3.2: C_p vs λ at V_∞ =10 m/s

λ	SST k-ω model (Re=10^6)		Laminar model (Re=5000)	Solidity with 6 Blades, (Re=10^6)
	D = 2 m.	D = 1 m.	D = 0.1365 m.	D = 2 m.
1	0.004	0.0027	-5.03	0.1539
2	-0.007	-0.0054	-1.75	0.216
3	0.263	0.267	-6.25	0.33
4	0.325	0.354	-6.02	-0.68
5	0.093	0.087	-11	-2.48

CHAPTER 4

CONCLUSIONS AND RECOMMENDATIONS

4.1 Summary

In the present study, a 2-D unsteady model of a vertical axis wind turbine comprising three rotating symmetric airfoils (NACA0018) has been designed with the consideration of a near wake. The flow around the wind turbine is simulated using ANSYS FLUENT 12.0.16 at Reynolds number of 10^6. ICEM CFD is used as a preprocessor to generate hexahedral grid and sliding mesh technique is implemented to create a moving mesh. SST k- ω Turbulence model is employed for the analysis and simulation is set to run at several tip speed ratios ranging from 1 to 5. Variation of C_p as a function of λ is then observed by plotting a graph between them. An appropriate validation is made by comparing CFD results with the experimental results by Claessens (2006). Maximum $C_p = 0.34$ is obtained at $\lambda = 3.8$. In addition, the effect of rotor diameter on VAWT's performance is also investigated. In this regard, rotor diameter is halved but the angular velocity is doubled to keep the tip speed ratio constant. Furthermore, theory behind leading edge separation bubble is proposed with the application of Laminar viscous model at low Reynolds number. Effect of solidity on C_p is also included in this thesis for a six bladed turbine.

4.2 Conclusions

The following conclusions are drawn on the basis of results obtained from 2-D CFD simulations of a VAWT as shown in previous chapter:

- Tip speed ratio is one of the influential factors on which coefficient of performance of a wind turbine depends.

- Depending on the type of airfoil used, every wind turbine has a particular range of operating tip speed ratios at which, turbine produces positive power output and for the rest of the values of λ it goes negative. In general a VAWT with fixed pitch blades is unable to start by itself. The major problem with the straight-bladed VAWT is the negative C_p at low tip speed ratios. A positive C_p shows that the turbine is able to rotate independently and produce power, whereas a negative C_p means the turbine needs extra power to be able to rotate.

- $C_{p,max} = 0.34$ is achieved at $\lambda = 3.8$ for a 3 bladed VAWT whereas for a 6 bladed VAWT $C_{p,max} = 0.39$ is achieved at comparatively lower value of λ that is 2.8.

- Influence of rotor diameter on the aerodynamic performance of a VAWT has been investigated and found that C_p remains almost constant at the same value of λ ranging from 1-5, this is due to the fact that the ratio of chord length and rotor radius (i. e. c/R) were kept the same in both the cases.

- For Laminar flow at low Reynolds number C_p was found to be low due to the presence of leading edge separation bubble and reduced lift-to-drag ratio.

- In order to increase C_p of a VAWT at low Reynolds numbers (e. g. small VAWT), different blade geometry (e. g. cambered) and different propulsion mechanism (inspired by insect flights) are needed.

- Influence of solidity was explored by involving six blades for the simulation and it was concluded that blockage effect increases with the increase in number of blades which causes lower entrance velocity and hence leads to higher torque generation. Maximum C_p is obtained at relatively lower value of λ as compared

to 3 bladed VAWT. It requires comparatively large torque to produce same amount of C_p.

4.3 Recommendations For The Future Work

- 3-D model of a VAWT can be proposed in the future studies to account for the tip vortices and rotor arms. The 2-D CFD simulation does not include the effects of the end tip vortices present on the real wind turbine and that is why, 2D simulations shows a significantly increased performance compared to the 3D simulations. Furthermore, the other reason for an overestimated numerical value of C_p of 2-D calculations as compared to 3-D could be the absence of rotor arms in 2-D simulations.

- In lieu of having a blade fixed to the rotor arm, a flapping or plunging mechanism can be provided which will help reducing the condition of a dynamic stall. It is the same phenomena used by insects.

BIBLIOGRAPHY

[1] Abbott, Ira H., and Von Doenhoff, Albert E., "Theory of Wing Sections: Including a Summary of Airfoil Data, Section 4.2", Dover Publications Inc., New York, 1959, Standard Book Number 486-60586-8.

[2] Ansari, S. A., Zbikowski, R. and Knowles, K., "Non-Linear Unsteady Aerodynamic Model For Insect-like Flapping Wings in the Hover. Part 1: Methodology and Analysis", Journal of Aerospace Engineering, 2006, Vol. 220, pp. 61-83.

[3] Birch, M. J. and Dickinson, H., "Spanwise Flow and the Attachment of the Leading-Edge Vortex on Insect Wings", Nature, 2001, Vol. 412, pp. 729-733.

[4] Bragg, G. M., and Schmidt, W. L., "Performance Matching and Optimization of Wind Powered Water Pumping Systems", Energy Conversion, 1978, Vol. 19, pp. 33-39.

[5] Cetin, N. S., Yurdusev, R. A., and Ozdemir, A., "Assesment of Optimum Tip Speed Ratio of Wind Turbines", Mathematical and Computational Applications, 2005, Vol. 10, pp. 147-154.

[6] Chen, W. and Zhou, C. Y., "Application of Numercal Simulation to Obtain the Optimization Pitch Angle for VAWT", IEEE, 2009, pp. 4244-4702.

[7] Claessens, M. C., "The Design and Testing of Airfoils for Application in Small Vertical Axis Wind Turbines", MS Thesis, 2006, Delft University of Technology.

[8] Darrieus, G.J.M., "Turbine Having Its Rotating Shafts Transverse to the Flow of the Current", United States Patent 1835018, 1931, pp. 1-4.

[9] Ellington, C. P., Berg, C. V. D., Willmott, A. P. and Thomas, A. L. R., "Leading-Edge Vortices in Insect Flight", Nature, 1996, Vol. 384, pp. 626-630.

[10] Ferreira, C. J. S., "The Near Wake of the VAWT - 2D and 3D Views of the VAWT Aerodynamics", PhD Dissertation, 2009, Delft University of Technology, The Netherlands.

[11] Guerri, O., Sakout A. and Bouhadef, K., "Simulations of the Fluid Flow Around a Rotating Vertical Axis Wind Turbine", Wind Engineering, 2007, Vol. 31, pp. 149-163.

[12] Howell, R., Qin, N., Edwards, J. and Durrani, N., "Wind Tunnel and Numerical Study of a Small Vertical Axis Wind Turbine", Renewable Energy, 2009, Vol. 35, pp. 412-422.

[13] Hover, F., Haugsdal, O. and Triantafyllou, M. S., "Effect of Angle of Attack Profiles in Flapping Foil Propulsion", Journal of Fluids and Structures, 2004, Vol. 19, pp. 37-47.

[14] Islam, M., Ting, D. SK., and Fartaj, A., "Aerodynamic Models for Darrieus-type Straight-Bladed Vertical Axis Wind Turbines", Renewable and Sustainable Energy Reviews, 2006, Vol. 12, pp. 1087-1109.

[15] Lee, J. S., Kim, C. and Kim, K. H., "Design of a Flapping Airfoil for Optimal Aerodynamic Performance in Low-Reynolds Number Flows", AIAA Journal, 2006, Vol. 44, pp. 1960-1972.

[16] Marini, M., Massardo, A. and Satta, A., "Performances of Vertical Axis Wind Turbines With Different Shapes", Journal of Wind Engineering and Industrial Aerodynamics, 1992, Vol. 39, pp. 83-93.

[17] Menter, F. R., "Two-Equation Eddy-Viscosity Turbulence Models for Engineering Applications", AIAA Journal, 1994, Vol. 32, pp. 1598-1605.

[18] Read, D. A., Hover, F. S. and Triantafyllou, M. S., "Forces on Oscillating Foils for Propulsion and Maneuvering", Journal of Fluids and Structures, 2002, Vol. 17, pp. 163-183.

[19] Sane, S. P. and Dickinson, M. H., "The Control of Flight Force by a Flapping Wing: Lift and Drag Production", The Journal of Experimental Biology, 2001, Vol. 204, pp. 2607- 2626.

[20] Sane, S. P. and Dickinson, M. H., "The Aerodynamic Effects of Wing Rotation and a Revised Quasi-Steady Model of Flapping Flight", The Journal of Experimental Biology, 2002, Vol. 205, pp. 1087-1096.

[21] Shyy, W. and Liu, H., "Flapping Wings and Aerodynamic Lift: The Role of Leading-Edge Vortices", AIAA Journal, 2007, Vol. 45, pp. 2817-2819.

[22] Shyy, W., Trizila, P., Kang, C. K. and Aono, H., "Can Tip Vortices Enhance Lift of a Flapping Wing?", AIAA Journal, 2009, Vol. 47, pp. 289-293.

[23] Tang, J., Viieru, D. and Shyy, W., "A Study of Aerodynamic of Low Reynolds Number Flexible Airfoils", 37th AIAA Fluid Dynamics Conference and Exhibit, 2007, Florida.

[24] Tay, W. B. and Lim, K. B., "Analysis of Non-Symmetrical Flapping Airfoils", Acta Mechanica Sinica, 2009, Vol. 25, pp. 433-450.

[25] Wang, Z. J., "Two Dimensional Mechanism for Insect Hovering", Physical review letters, 2000, Vol. 85, pp. 2216-2219.

Additional References

[26] ANSYS FLUENT 12.0.16 manual, 2009.

[27] Quiet Revolution Ltd, "Gallery", <http://www.quietrevolution.com/index.htm>.

[28] White, F. M., "Viscous Fluid Flow," (2005), McGraw-Hill Companies, 3rd edition.

[29] World Wind Energy Association, (2008), <http://www.wwindea.org/home/index.php?option=com_content&task=view&id=266&Itemid=43>.

APPENDIX A

Steps involved in post-processing of VAWT using ANSYS FLUENT 12.0.16

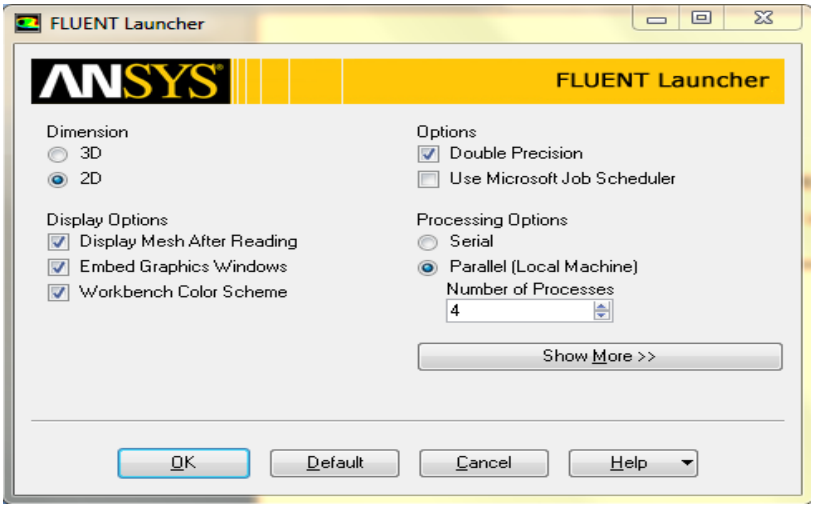

Figure 1: Fluent launcher panel

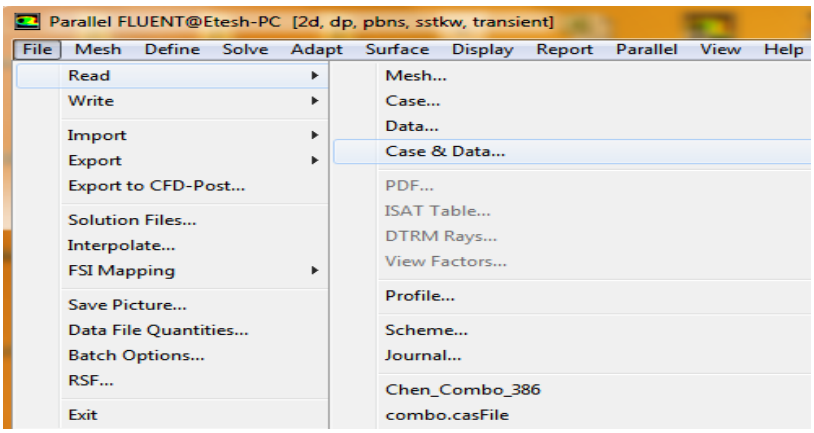

Figure 2: Read-case-data panel

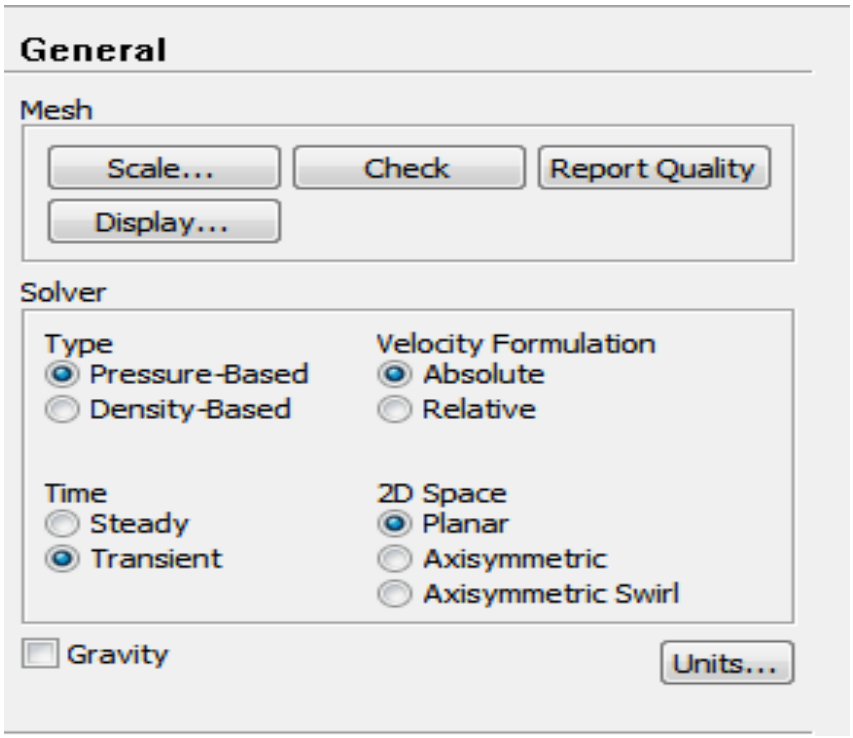

Figure 3: General panel

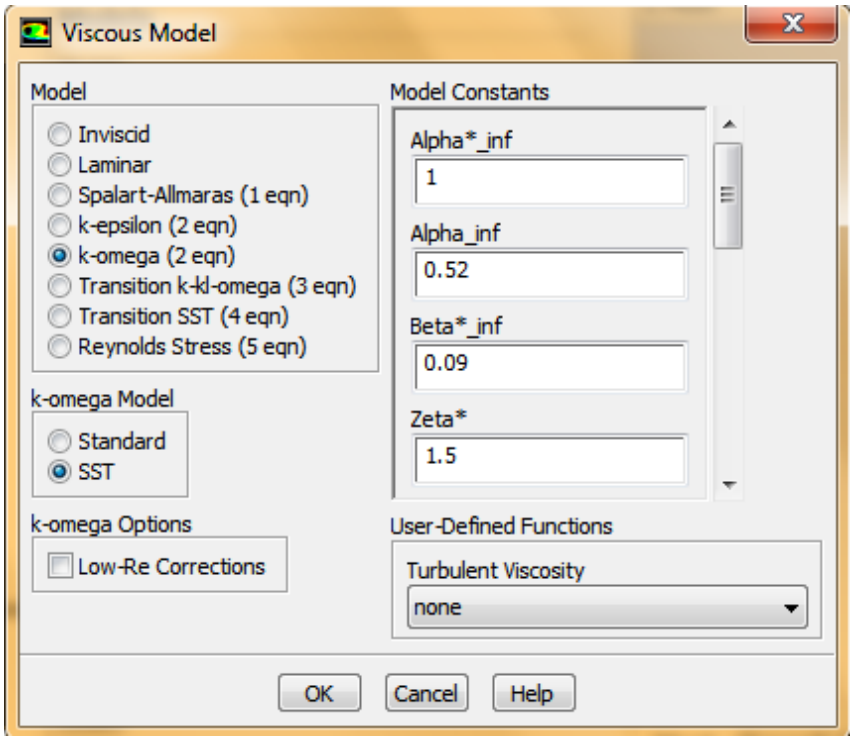

Figure 4: Model panel

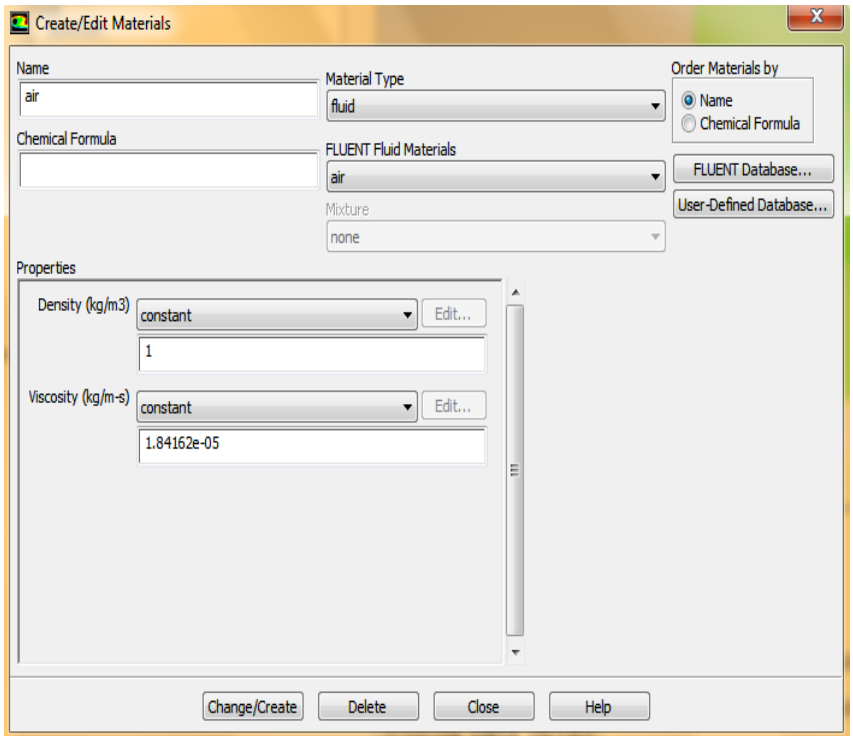

Figure 5: Materials panel

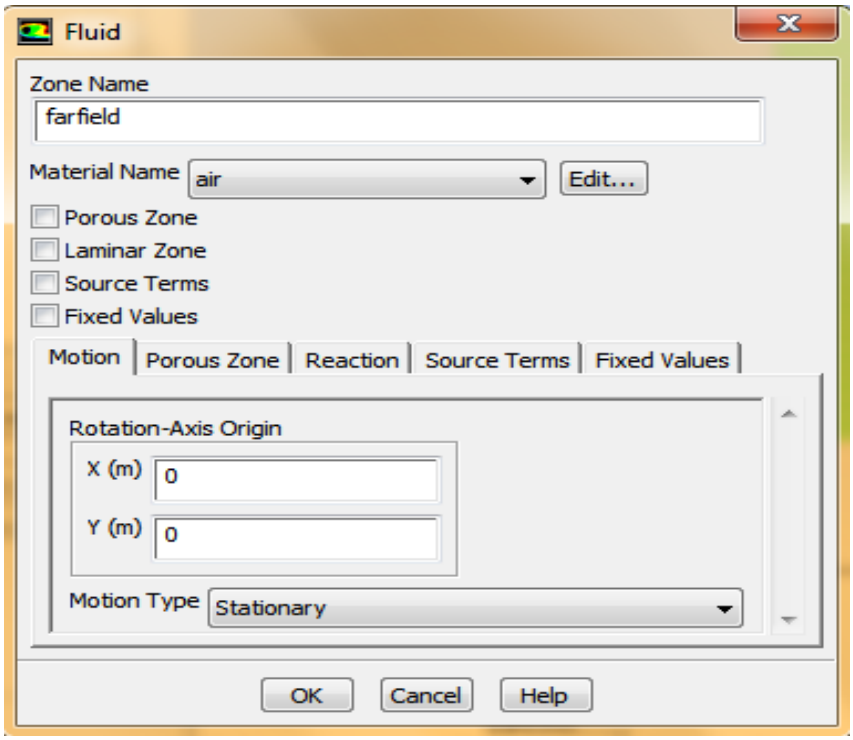

Figure 6: Cell zone conditions panel

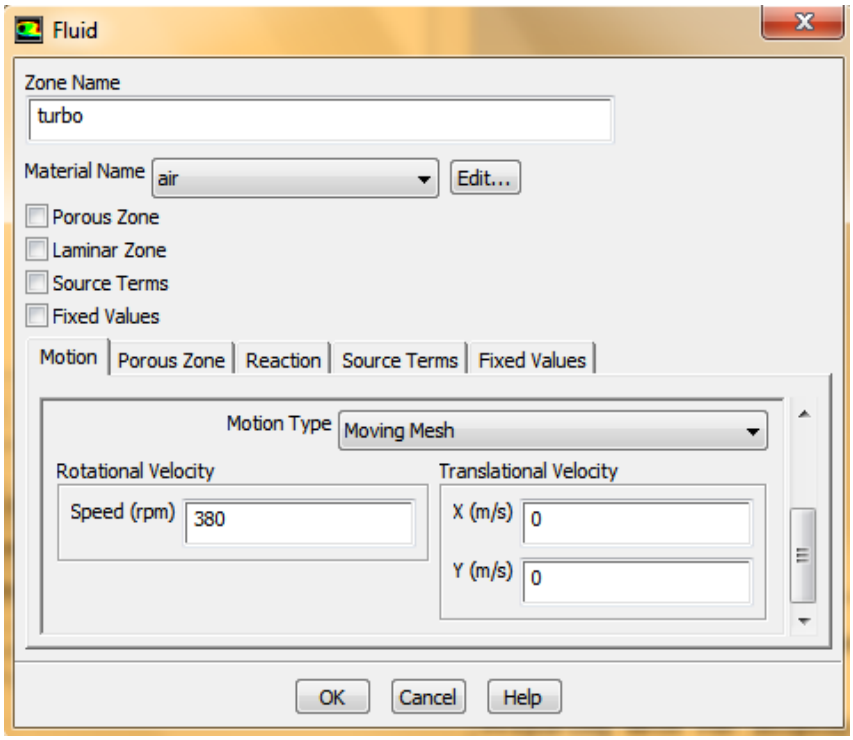

Figure 7: Cell zone conditions panel

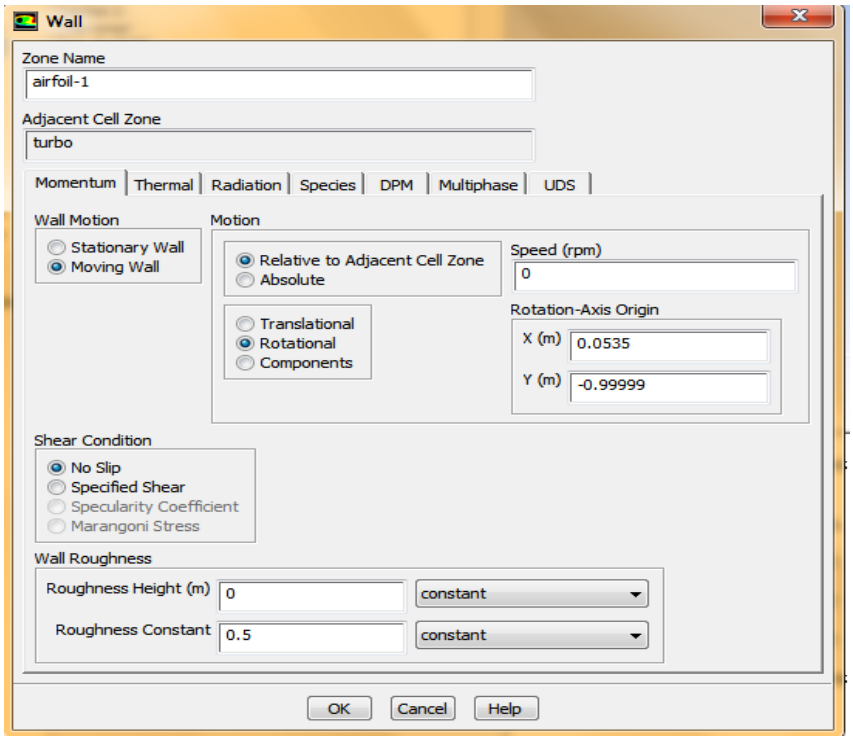

Figure 8: Boundary conditions panel

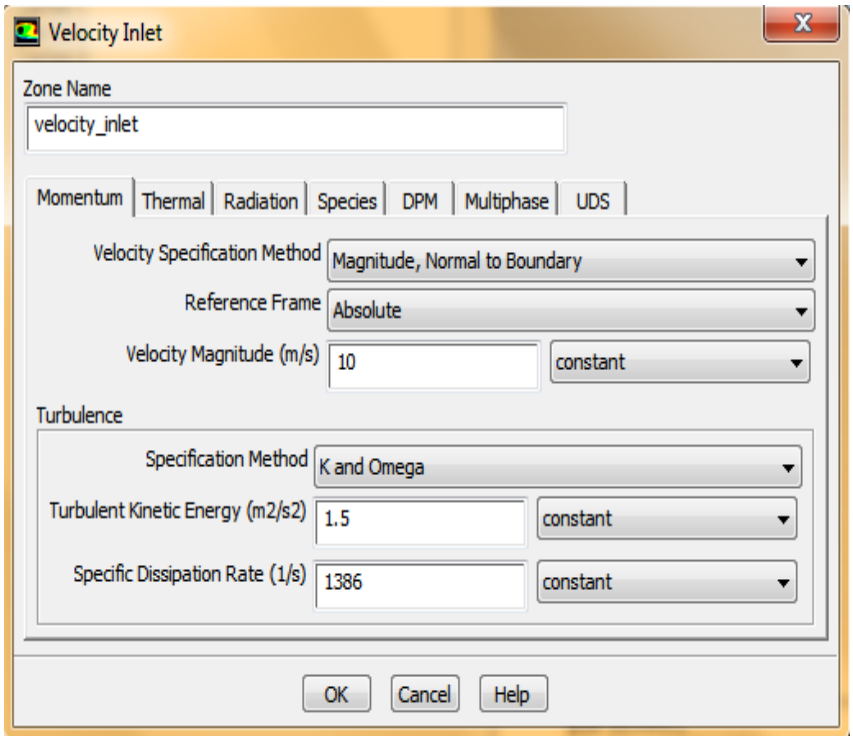

Figure 9: Boundary conditions panel

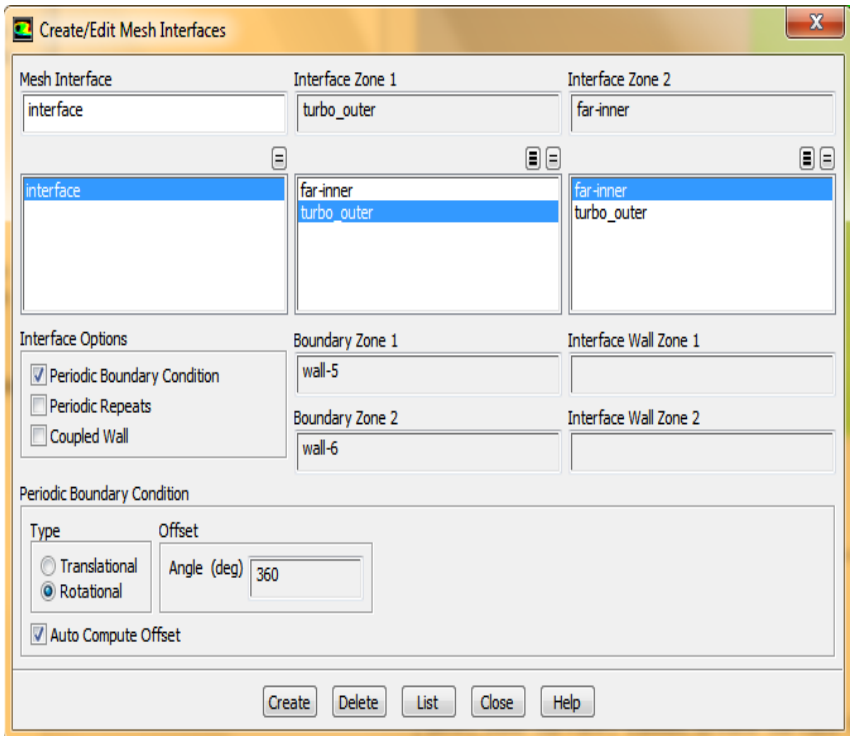

Figure 10: Mesh interface panel

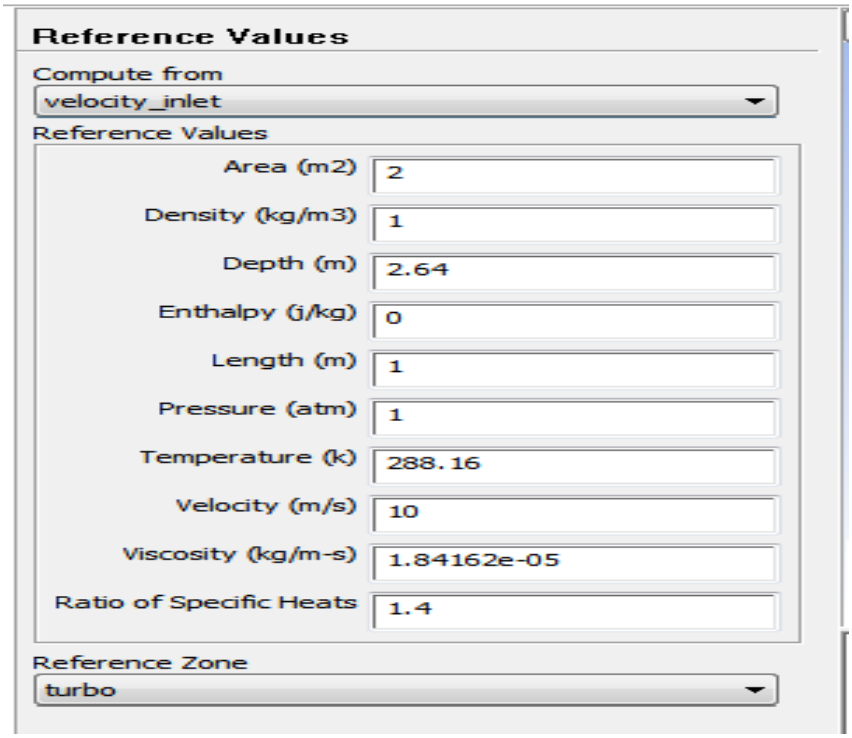

Figure 11: Reference values panel

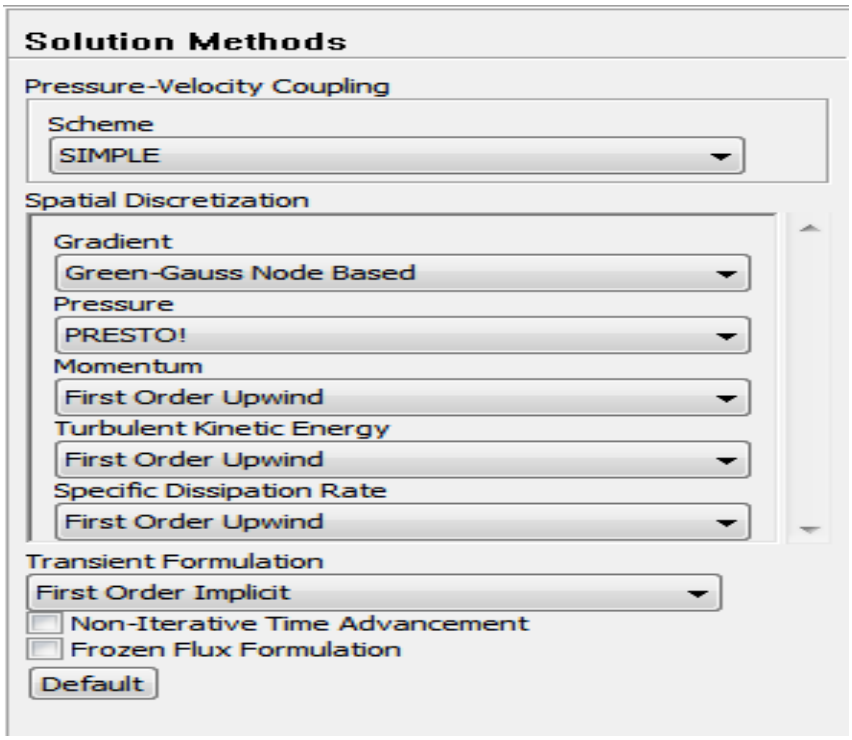

Figure 12: Solution methods panel

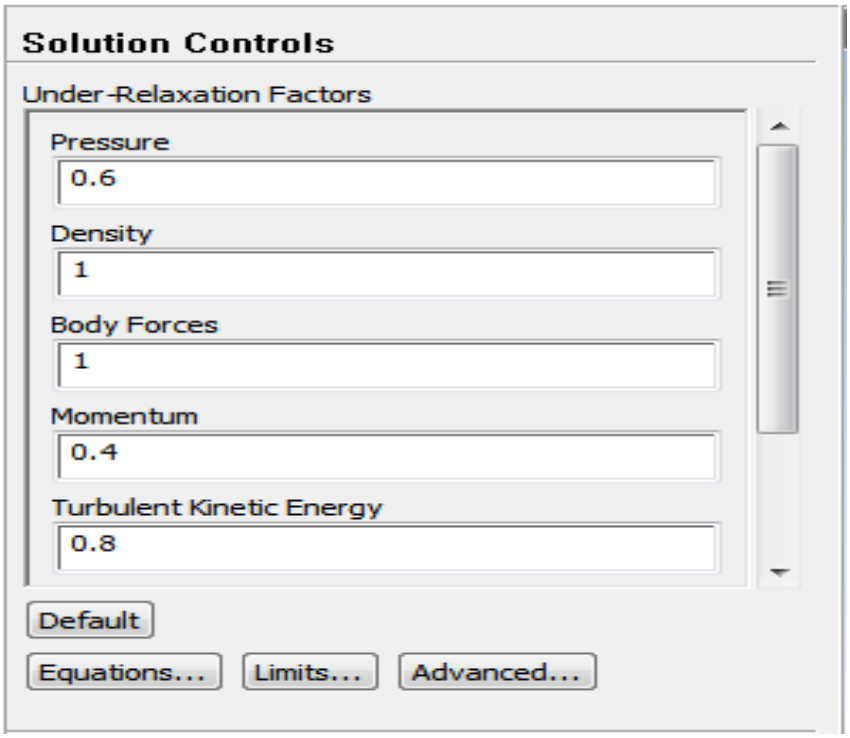

Figure 13: Under relaxation factor panel

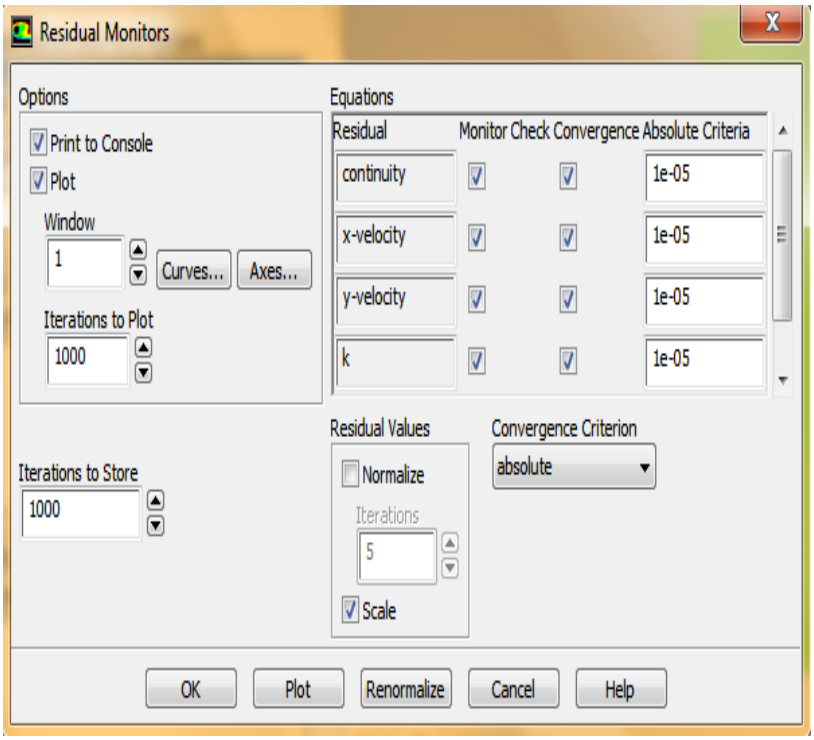

Figure 14: Monitors residual panel

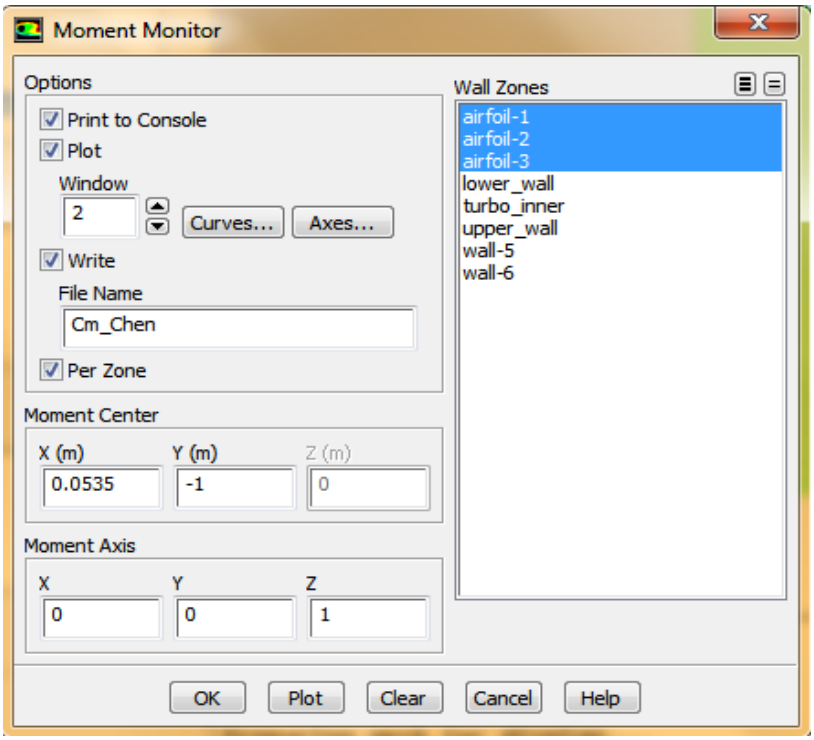

Figure 15: Monitors moment panel

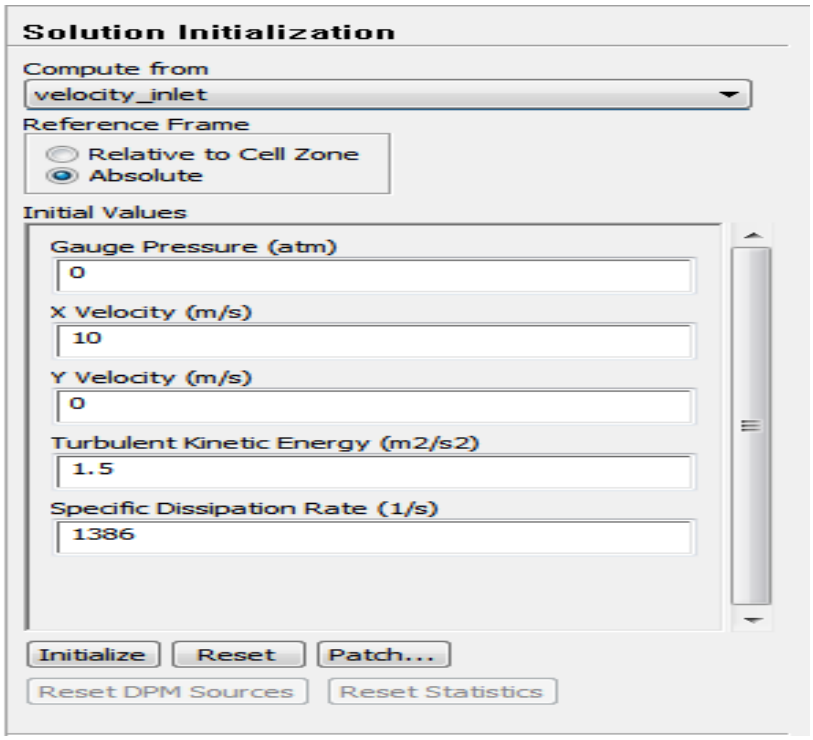

Figure 16: Solution initialization panel

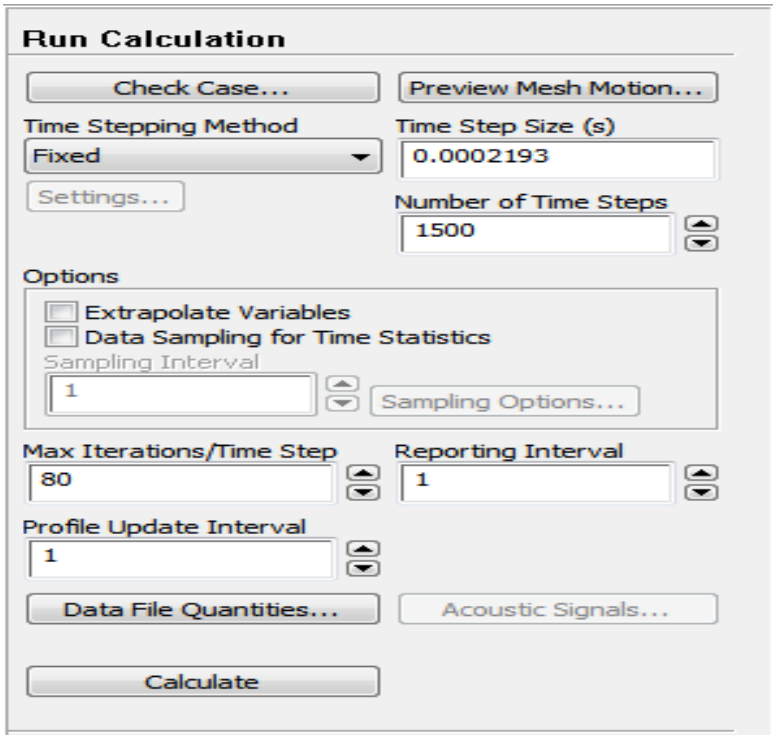

Figure 17: Calculation activities panel

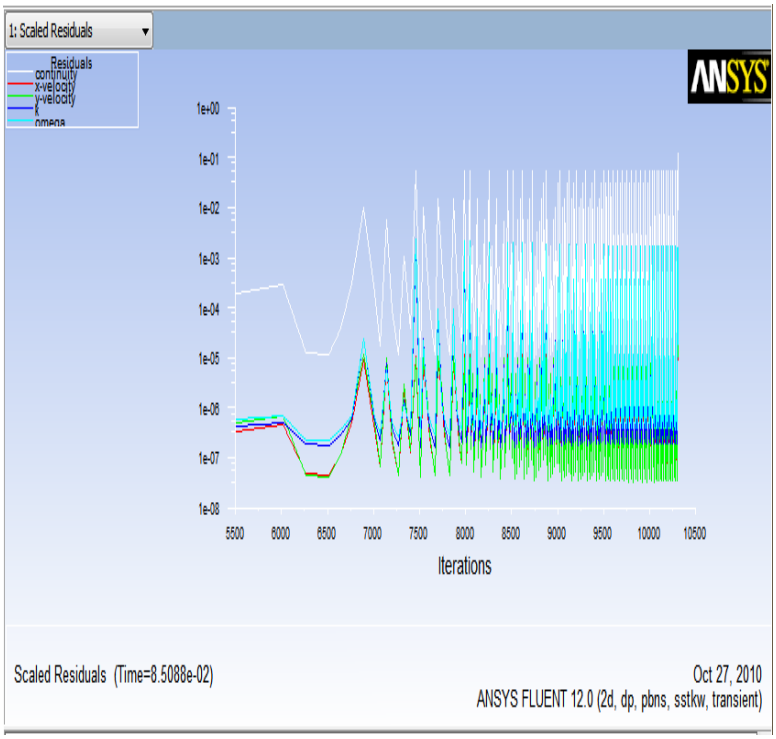

Figure 18: Scaled residuals

APPENDIX B

In this appendix the coordinates of the NACA 0018 Airfoil profiles are given. These are the coordinates used for the 2-D unsteady simulations.

Table 1: NACA 0018 Coordinates

x/c	y/c	z/c	x/c	y/c	z/c
1	0	0	0.5	-0.0789	0
0.999	-0.0002	0	0.4686	-0.0818	0
0.9961	-0.0008	0	0.4373	-0.0843	0
0.9911	-0.0019	0	0.4063	-0.0864	0
0.9843	-0.0033	0	0.3757	-0.088	0
0.9755	-0.0051	0	0.3455	-0.0891	0
0.9649	-0.0073	0	0.3159	-0.0897	0
0.9524	-0.0099	0	0.2871	-0.0898	0
0.9382	-0.0127	0	0.2591	-0.0893	0
0.9222	-0.0159	0	0.2321	-0.0882	0
0.9045	-0.0193	0	0.2061	-0.0865	0
0.8853	-0.023	0	0.1813	-0.0842	0
0.8645	-0.0268	0	0.1577	-0.0813	0
0.8423	-0.0308	0	0.1355	-0.0778	0
0.8187	-0.0349	0	0.1147	-0.0737	0
0.7939	-0.0392	0	0.0955	-0.0691	0
0.7679	-0.0434	0	0.0778	-0.0639	0
0.7409	-0.0478	0	0.0618	-0.0583	0
0.7129	-0.0521	0	0.0476	-0.0522	0
0.6841	-0.0564	0	0.0351	-0.0457	0
0.6545	-0.0606	0	0.0245	-0.0388	0
0.6243	-0.0646	0	0.0157	-0.0316	0
0.5937	-0.0686	0	0.0089	-0.0241	0
0.5627	-0.0723	0	0.0039	-0.0163	0
0.5314	-0.0757	0	0.001	-0.0083	0

x/c	y/c	z/c	x/c	y/c	z/c
0	0	0	0.5	0.0789	0
0.001	0.0083	0	0.5314	0.0757	0
0.0039	0.0163	0	0.5627	0.0723	0
0.0089	0.0241	0	0.5937	0.0686	0
0.0157	0.0316	0	0.6243	0.0646	0
0.0245	0.0388	0	0.6545	0.0606	0
0.0351	0.0457	0	0.6841	0.0564	0
0.0476	0.0522	0	0.7129	0.0521	0
0.0618	0.0583	0	0.7409	0.0478	0
0.0778	0.0639	0	0.7679	0.0434	0
0.0955	0.0691	0	0.7939	0.0392	0
0.1147	0.0737	0	0.8187	0.0349	0
0.1355	0.0778	0	0.8423	0.0308	0
0.1577	0.0813	0	0.8645	0.0268	0
0.1813	0.0842	0	0.8853	0.023	0
0.2061	0.0865	0	0.9045	0.0193	0
0.2321	0.0882	0	0.9222	0.0159	0
0.2591	0.0893	0	0.9382	0.0127	0
0.2871	0.0898	0	0.9524	0.0099	0
0.3159	0.0897	0	0.9649	0.0073	0
0.3455	0.0891	0	0.9755	0.0051	0
0.3757	0.088	0	0.9843	0.0033	0
0.4063	0.0864	0	0.9911	0.0019	0
0.4373	0.0843	0	0.9961	0.0008	0
0.4686	0.0818	0	0.999	0.0002	0

VITA

ETESH VAISHNAV

Candidate for the Degree of

Master of Science

Thesis: AN INVESTIGATION ON THE AERODYNAMIC PERFORMANCE OF A VERTICAL AXIS WIND TURBINE

Major Field: Mechanical and Aerospace Engineering

Biographical:

Personal Data: Born in Bilaspur, India on April 22^{nd}, 1985.

Education:

Received Bachelor of Engineering degree in Mechanical Engineering from Bhilai Institute of Technology, Durg, India, 2007.
Completed the requirements for the degree of Master of Science with a major in Mechanical and Aerospace Engineering from Oklahoma State University in December 2010.

Experience:

Worked as a Graduate Research Student under the aegis of Dr. Khaled A. Sallam in the area of CFD Simulation of a Vertical Axis Wind Turbine (Aug 2009- Dec 2010).
Employed as a Teaching Assistant for Mechanical and Aerospace Engineering, Oklahoma State University (Aug 2010- Dec 2010).
Employed as a Graduate Research Assistant for Agricultural Economics, Oklahoma State University (Jan 2009- May 2009).

Name: Etesh Vaishnav Date of Degree: December, 2010

Institution: Oklahoma State University Location: Stillwater, Oklahoma

Title of Study: AN INVESTIGATION ON THE AERODYNAMIC PERFORMANCE OF A VERTICAL AXIS WIND TURBINE

Pages in Study: 76 Candidate for the Degree of Master of Science

Major Field: Mechanical and Aerospace Engineering

Scope and Method of Study:

The two dimensional unsteady flow around a vertical axis wind turbine (VAWT) comprising three rotating symmetric airfoils (NACA0018) was studied numerically with the consideration of the near wake. The flow around the wind turbine was simulated using ANSYS FLUENT 12.0.16 at Reynolds number of 10^6. ICEM CFD was used as a pre-processor to generate hexahedral grid and arbitrary sliding mesh technique was implemented to create a moving mesh. SST k- ω turbulence model was employed for the analysis and simulation was set to run at several tip speed ratios ranging from 1 to 5. The variation of the performance coefficient (C_p) as a function of tip speed ratio (λ) was investigated by plotting a graph between them. A validation was made by comparing CFD results with experimental results. Maximum C_p of 0.34 was obtained at λ of 3.8. In addition, the effect of the rotor diameter on the VAWT's performance was investigated. In this regard, rotor diameter was halved and the angular velocity was doubled to keep the tip speed ratio constant. Furthermore, the effect of laminar boundary layer separation on C_p of a VAWT was studied by comparing the results of Laminar viscous model and RANS turbulence model. Apart from that, the effect of solidity on C_p was investigated by comparing the C_p obtained from six bladed turbine with the three bladed turbine.

Findings and Conclusions:

Influence of rotor diameter on the aerodynamic performance of a VAWT was investigated and found that C_p remained almost constant at the same value of λ ranging from 1 to 5. This was due to the fact that the ratio of the chord length and the rotor radius were kept the same in both cases. For Laminar flow at low Reynolds number, C_p was found to be low due to the presence of leading edge separation bubble and reduced lift-to-drag ratio. Therefore, in order to increase C_p of a VAWT at low Reynolds numbers (e. g. small VAWT), different blade geometry (e. g. cambered) and different propulsion mechanism are needed. Influence of solidity was explored by involving six blades for the simulation and it was concluded that blockage effect increased with the increase in number of blades which caused the maximum C_p to be obtained at a relatively lower value of λ as compared to three bladed VAWT.

ADVISOR'S APPROVAL: Khaled A. Sallam